Seawater-Fluid Composition Records From Molybdenum Isotopes of Sequentially Extracted Phases of Seep Carbonate Rocks

Zice Jia[1,2], Yu Hu[1] , Germain Bayon[3], Jörn Peckmann[4] , Xudong Wang[1], Shanggui Gong[1], Jie Li[5] , Harry H. Roberts[6], Duofu Chen[1,2] , and Dong Feng[1,2]

[1]College of Marine Sciences, Shanghai Ocean University, Shanghai, China, [2]Laboratory for Marine Mineral Resources, Qingdao National Laboratory for Marine Science and Technology, Qingdao, China, [3]CNRS, Ifremer, Geo-Ocean, University of Brest, Plouzané, France, [4]Institute for Geology, Center for Earth System Research and Sustainability, Universität Hamburg, Hamburg, Germany, [5]State Key Laboratory of Isotope Geochemistry, Guangzhou Institute of Geochemistry, Chinese Academy of Sciences, Guangzhou, China, [6]Coastal Studies Institute, College of the Coastal and Environment, Louisiana State University, Baton Rouge, LA, USA

Abstract Authigenic molybdenum (Mo_{auth}) in marine sediments holds great potential to archive the Mo isotopic composition of seawater and biogeochemical processes. However, the factors that control authigenic Mo isotope ($\delta^{98}Mo_{auth}$) distribution patterns remain poorly constrained. Here, we report Mo abundances and $\delta^{98}Mo$ compositions for bulk-rock (*bulk*) and sequentially extracted fractions—including total authigenic (*auth*; i.e., non-lithogenic fraction), carbonate (*carb*), iron and manganese oxyhydroxides, pyrite (*py*), and organic fractions (*OM*)—of authigenic carbonates recovered from various hydrocarbon seep sites in the Gulf of Mexico and the South China Sea. Extracted pyrite fractions exhibit Mo contents varying from 0.1 to 23.4 µg/g and generally dominate the Mo budget of seep carbonate rocks. Our data indicate large ranges of $\delta^{98}Mo_{bulk}$ and $\delta^{98}Mo_{auth}$ values relative to NIST 3134 (0.25‰), varying from 1.02 to 1.98‰ (*n* = 4) and from 0.15 to 3.07‰ (*n* = 34), respectively. The difference in $\delta^{98}Mo$ values between carbonate and pyrite fractions of seep carbonate rocks formed under sulfidic conditions increases with higher Mo_{auth} contents, suggesting a control of dissolved hydrogen sulfide concentrations on Mo isotope fractionation during carbonate precipitation. Compared with $\delta^{98}Mo_{auth}$ and $\delta^{98}Mo_{py}$, $\delta^{98}Mo_{carb}$ of seep carbonate rocks formed under sulfidic conditions shows a relatively narrow range with an average of $1.98 \pm 0.31‰$ (1 SD; *n* = 10), providing constraints on the $\delta^{98}Mo$ composition of seawater in the course of Earth history. Overall, our findings show that the $\delta^{98}Mo$ composition of sequentially extracted phases of carbonate-rich sedimentary rocks can provide insights into seawater-sediment interactions and biogeochemical pathways of Mo during early diagenesis.

Plain Language Summary Sulfate reduction has created widespread euxinic conditions in the water column of ancient oceans and prevalent sulfidic conditions in subseafloor pore-water environments of the modern ocean. Ancient seawater $\delta^{98}Mo$ compositions have been considered to reflect the overall extent of oxic versus euxinic conditions of the global ocean, highlighting the importance of a robust reconstruction of the marine Mo isotope inventory largely unaffected by diagenesis. Under sulfidic conditions, the seawater $\delta^{98}Mo$ value can be archived by authigenic Mo in marine carbonate sediments formed during early diagenesis. However, the conditions of capturing the seawater $\delta^{98}Mo$ signature remain poorly constrained. Using a sequentially chemical leaching procedure, we investigated Mo contents and isotopic compositions of different fractions of modern seafloor seep carbonate rocks. Our results show that a $\delta^{98}Mo$ average value of $1.98 \pm 0.31‰$ (1 SD; *n* = 10) of the carbonate mineral phase results from small or no Mo isotope fractionation during near-quantitative authigenic Mo sequestration under sulfidic conditions, potentially capturing seawater $\delta^{98}Mo$. Our study shows that $\delta^{98}Mo$ of sequentially extracted phases of sedimentary carbonate rocks is a robust tool to constrain seawater and pore fluid properties.

1. Introduction

The molybdenum isotope ($\delta^{98}Mo$) composition (i.e., the $^{98}Mo/^{95}Mo$ ratio relative to NIST SRM 3134 = +0.25‰; Nägler et al., 2014) of organic-rich sediments has been widely used to reconstruct the redox state of seawater in the geological past (e.g., Arnold et al., 2004; X. Chen et al., 2015; Cheng et al., 2020; Dickson et al., 2014; Goldberg et al., 2016; O'Sullivan et al., 2022). Molybdenum is highly soluble in oxic seawater, with a long

residence time of ca. 440 ka (Colodner et al., 1995; Emerson & Huested, 1991; Miller et al., 2011). Under oxic aqueous conditions, dissolved Mo has a relatively strong affinity to iron and manganese oxides, resulting in preferential adsorption of isotopically light Mo onto iron and manganese oxides with a fractionation of 0.8–3.2‰ relative to seawater (e.g., Barling & Anbar, 2004; Barling et al., 2001; S. Chen et al., 2022; Eroglu et al., 2020; Goldberg et al., 2009; Scholz et al., 2017; Siebert et al., 2003; Wasylenki et al., 2008). In contrast, dissolved Mo is much less soluble at high H_2S concentrations in strongly restricted basins, resulting in near-quantitative Mo sequestration in underlying sediments, hence without any significant Mo isotope fractionation relative to seawater (e.g., Gordon et al., 2009; Neubert et al., 2008; Siebert et al., 2003). Due to its long residence time and distinctive behavior under oxic versus euxinic conditions, one major advantage of using Mo in ancient sedimentary archives of seawater chemistry is that $\delta^{98}Mo$ values obtained for any given site can be used to infer the integrated redox condition of the global ocean at the time of deposition (e.g., Neubert et al., 2008; Phillips & Xu, 2021; Poulson et al., 2006; Siebert et al., 2003).

The presence of dissolved hydrogen sulfide (H_2S) in the water column or pore waters promotes the conversion of molybdates (MoO_4^{2-}) to thiomolybdates ($MoS_{4-x}O_x^{2-}$; with $1 < x < 4$; e.g., Erickson & Helz, 2000; Helz et al., 1996, 2011; Zheng et al., 2000). The conversion from molybdates to thiomolybdates is highly effective and Mo can be quantitatively scavenged into sulfidic sediments above a threshold H_2S concentration of 11 μM (Erickson & Helz, 2000). A second threshold concentration of H_2S of approximately 100 μM has been proposed for Mo sequestration without iron, possibly as Mo-S or as particle-bound Mo (Helz et al., 2011; Zheng et al., 2000). Other studies have reported $\delta^{98}Mo$ values much lower than seawater in organic-rich sediments underlying euxinic bottom waters having H_2S concentrations lower than 11 μM (e.g., Arnold et al., 2004; Bura-Nakić et al., 2018; Goldberg et al., 2012; Poulson et al., 2006; Scholz et al., 2017). The occurrence of weakly euxinic water column conditions can hence compromise the use of $\delta^{98}Mo$ in ancient organic-rich sediments as a proxy for reconstructing past ocean redox conditions (Arnold et al., 2004; X. Chen et al., 2015; Kendall et al., 2017).

In contrast to ancient organic-rich sediments, ancient sedimentary carbonates are more common in the geological record, both spatially and temporally (Morse & Mackenzie, 1990; Shields & Veizer, 2002; Wilkinson & Walker, 1989). Previous investigations on carbonate-rich sedimentary rocks have suggested that non-skeletal carbonates may reliably archive the seawater $\delta^{98}Mo$ composition (Clarkson et al., 2020; Czaja et al., 2012; Voegelin et al., 2009, 2010). However, recent studies on carbonate-dominated sediments from modern marine environments have found that authigenic Mo enrichments in anoxic carbonate-rich sediments generally result from early diagenesis in the presence of sulfidic conditions in sub-seafloor environments (Bura-Nakić et al., 2020; Romaniello et al., 2016). While the acquisition of seawater $\delta^{98}Mo$ signatures during carbonate precipitation appears to be favored under sulfidic conditions (Bura-Nakić et al., 2020; Romaniello et al., 2016), the detailed processes behind the preservation of seawater $\delta^{98}Mo$ during the incorporation of dissolved pore water Mo into carbonate-rich sediments are still poorly constrained. A recent study has reported some $\delta^{98}Mo$ data for seep carbonate rocks formed under sulfidic conditions at marine methane seeps, yielding an average $\delta^{98}Mo$ of 1.90‰ ($n = 5$), corresponding to an offset of −0.4‰ relative to seawater (Lin et al., 2021). Based on these results, it was suggested that seep carbonate rocks have the potential to preserve seawater Mo isotopic composition with relatively minor offsets. However, the factors controlling the distribution of $\delta^{98}Mo$ in authigenic carbonate rocks at methane seeps remain poorly understood. Additional information is required to characterize the degree of Mo isotopic fractionation between the pore fluid and solid phase and to further understand the behavior of Mo isotopes during early diagenesis. Because negligible Mo isotopic fractionation is thought to occur during calcite precipitation (X. Chen et al., 2021), the $\delta^{98}Mo$ composition of the carbonate phase in seep carbonate rocks is expected to faithfully preserve the $\delta^{98}Mo$ signature of the pore waters from which carbonate minerals precipitated. The $\delta^{98}Mo$ composition of different components of seep carbonate rocks is therefore expected to be useful in the determination of Mo isotopic fractionation during early diagenesis.

Moderate-to-significant Mo enrichments in sediments or authigenic carbonates at submarine hydrocarbon seeps have been observed with Mo contents varying from ~1 to 118 μg/g (e.g., F. Chen et al., 2016; Deng et al., 2020; Guan et al., 2022; Hu et al., 2014; Lin et al., 2021; Sato et al., 2012; Smrzka et al., 2020). At seeps, carbonate precipitation typically occurs in close association with sulfate-driven anaerobic oxidation of methane, which produces high alkalinity levels in surrounding pore waters (e.g., Boetius et al., 2000; Peckmann & Thiel, 2004). In this study, we have analyzed a suite of authigenic carbonates from various seep sites ($n = 9$; Figure 1) from the Gulf of Mexico and the South China Sea (Feng & Chen, 2015; Huang et al., 2020; Roberts et al., 2010; Sun et al., 2020, 2021; Tong et al., 2019). The studied seep carbonate rocks
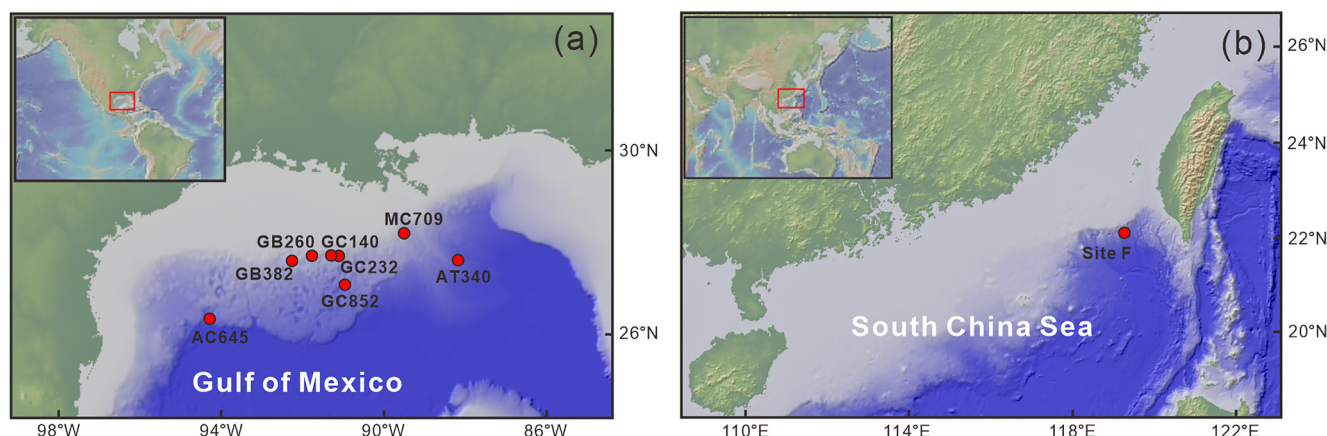
Figure 1. Maps showing the study areas and sampling sites. Seep carbonate rocks were recovered at eight sites from the (a) Gulf of Mexico and at one site from the (b) South China Sea.

were analyzed for their mineral and $\delta^{13}C$ and $\delta^{18}O$ compositions, and element abundances (including carbon, sulfur, and trace elements). Additionally, Mo contents and $\delta^{98}Mo$ compositions were determined on separate phases, including bulk-rock and total authigenic fractions, as well as on sequentially extracted fractions of carbonate, iron and manganese oxide, pyrite, and organic matter, respectively. The purpose of this work is to identify the factors controlling $\delta^{98}Mo$ distribution patterns in seep carbonate rocks, with the aim of further constraining the behavior of Mo isotopes during early diagenesis for a better application in paleoenvironmental reconstructions.

2. Materials and Methods

2.1. Materials

The seep carbonate rock samples used for this study are listed in Table 1. After collection and cleaning with deionized water, most samples ($n = 23$) were ground to <200 mesh using an agate mortar. A few powdered samples ($n = 7$) were also obtained using a hand-held dental drill. The samples were subdivided into three groups based on their mineralogical composition and relative proportions of low-Mg calcite (LMC), aragonite, and high-Mg calcite (HMC; see Section 3.1).

2.2. Analytical Methods

2.2.1. Carbonate Mineralogy

Bulk mineralogy and relative abundance of carbonate minerals were determined by X-ray diffraction (XRD) using a LabX XRD-6100 diffractometer equipped with a diffracted beam graphite monochromator using CuKα radiation at Shanghai Ocean University. Samples were scanned from 10° to 80° (2θ) at 0.02°/s with the X-ray source operated at 40 kV accelerating voltage and 30 mA current. The diverging, scattering, and receiving slits during scanning were 1°, 0.3°, and 1 mm, respectively. The relative abundances of carbonate minerals were quantified based on the (104) peak areas of LMC, HMC, and dolomite and the (111) peak area of aragonite using calibration curves (Greinert et al., 2001). The $MgCO_3$ content of carbonate minerals was calculated from the d[104]-shift using the average of the linear correlation according to Goldsmith et al. (1961) and Lumsden (1979). Calcite with <5 mol% $MgCO_3$, 5–20 mol% $MgCO_3$, and 36–50 mol% $MgCO_3$ were classified as LMC, HMC, and dolomite, respectively (Burton, 1993; Burton & Walter, 1991). Therefore, dolomite includes proto-dolomite and ordered dolomite (Burton, 1993). Petrographic observations were conducted using

Table 1
Sample and Site Information for Seep Carbonate Rocks in This Study

Sample ID	Site	Water depth (m)	References
1–2	GB260	460	Huang et al. (2020)
4, 6	GC140	260–510	Tong et al. (2019)
12	GB382	260–510	Tong et al. (2019)
13–16	AC645	2,240	Roberts et al. (2010)
17–21	GC232	570	Sun et al. (2020)
23–26	AT340	2,216	Roberts et al. (2010)
27-29, 31, 33	GC852	1,633	Roberts et al. (2010)
34, 35	MC709	680–700	Sun et al. (2021)
38, 40-43	Site F	1,120	Feng and Chen (2015)

optical microscopy. The microstructures of fresh carbonate rock fragments were examined using a scanning electron microscope (SEM) at Shanghai Ocean University.

2.2.2. Total Organic Carbon and Sulfur Contents and Carbon and Oxygen Isotope Compositions

Prior to carbon and sulfur content measurements, about 1 g powdered samples were acidified with 4 M HCl for 12 hr to remove carbonate minerals. The residue was centrifuged, thoroughly rinsed with deionized water, and finally freeze dried for further analysis. Because of preceding acidification, the analyzed carbon represents total organic carbon (TOC). Due to both the release of acid volatile sulfide during acidification and the presence of negligible organic sulfur in studied samples, the obtained sulfur contents correspond mainly to pyrite-bound sulfur (S_{py}). Contents of TOC and S_{py} were determined by a Vario EI-III Elemental Analyzer (EA) with an analytical precision of <2% at the Third Institute of Oceanography, State Oceanic Administration. For those LMC carbonates containing non-negligible amounts of barite (Huang et al., 2020; Sun et al., 2021), S_{py} contents were determined by chemical extraction using 6 N HCl and 1 M $CrCl_2$ solutions. The extraction was conducted in an O_2-free reaction vessel with continuous N_2 flow, and the released H_2S gas was trapped in $AgNO_3$ solution and precipitated as Ag_2S. Dried Ag_2S precipitates were weighed to obtain S_{py} contents. TOC and S_{py} contents are only available for samples ground with an agate mortar, while a few samples (ID 12, 16, 19, 24, 26, 31, 33) collected through micro-drilling were not analyzed for TOC and S_{py}.

For carbon and oxygen stable isotope analyses of carbonate phases in seep carbonate rocks, powdered samples were processed with 100% phosphoric acid at 70°C. The released CO_2 was analyzed using a Gasbench II-Delta V Advantage mass spectrometer at Shanghai Ocean University. The processed samples were firstly combusted to CO_2 using an EA. The released CO_2 was subsequently analyzed using a Delta V Advantage mass spectrometer at the Third Institute of Oceanography, State Oceanic Administration. Carbon and oxygen isotope values are reported using the δ notation relative to the Vienna-Pee Dee Belemnite standard with precision on the order of 0.1‰ (2SD) for both $δ^{13}C$ and $δ^{18}O$ values.

2.2.3. Trace Element Contents in Bulk-Rock and Total Authigenic Fractions

For trace element analysis of bulk-rock, about 50 mg of powdered samples were digested using ultrapure concentrated HNO_3 and HF (185°C; 36 hr) following the analytical procedure of Hu et al. (2014). The above solution was evaporated to dryness, and the residue was then completely dissolved using HNO_3 (135°C; 5 hr).

To determine trace element abundances in the non-lithogenic fraction of seep carbonate rock samples, about 50 mg of powdered samples were dissolved in a mixture of concentrated HNO_3 and HCl (*v/v* = 3) at 110°C for 24 hr. The non-lithogenic fraction of marine sediments or carbonates is typically referred to as the "authigenic" fraction (e.g., Bura-Nakić et al., 2020; Eroglu et al., 2020; He et al., 2021; Scholz et al., 2017; Voegelin et al., 2009), although some non-lithogenic components such as iron-manganese oxides and organic matter may not be *sensu stricto* authigenic (i.e., not formed in situ in the marine subsurface). Nevertheless, the non-lithogenic fraction of carbonate samples is still referred to as "authigenic" fraction herein for better comprehensibility, and includes carbonate, iron-manganese oxides, organic matter, and sulfide minerals. After centrifugation, the supernatant was evaporated to dryness, and the obtained residue was re-dissolved in HNO_3 prior to analysis. Trace element abundances in bulk-rock and total authigenic fractions of studied samples were determined using a Thermo Fisher iCAPRQ ICP-MS at Shanghai Ocean University or a Thermo Fisher X series 2 ICP-MS at Guizhou Tongwei Analytical Technology Co., Ltd. Certified reference materials (W-2a and BHVO-2) and a single standard solution of Mo were used for quality control. Precision and accuracy were better than 5% for Fe, Mn, and Mo.

2.2.4. Mo and Trace Element Contents in Sequentially Extracted Fractions

Sequentially chemical extraction was used to determine the abundances of Mo and other trace elements in different phases of seep carbonate rocks, namely carbonates, iron and manganese oxides, sulfides, and organic matter. First, about 300 mg of powdered sample was treated with 5% ultrapure acetic acid for 16 hr to remove carbonate minerals and extract carbonate-bound Mo (Rongemaille et al., 2011). Afterward, the iron and manganese oxide phases were dissolved using a solution of 0.5 M hydroxylamine HCl adjusted to pH 1.5 (16 hr) according to Tessier et al. (1979). Sulfide minerals, mainly pyrite, were subsequently dissolved by leaching with 3 M HNO_3 for 12 hr at room temperature (Chao & Sanzolone, 1977). Note that the use of up to 7 M HNO_3 at room temperature generally prevents extensive oxidation of organic matter (Han et al., 2009). Finally, organic compounds preserved

in seep carbonate rocks were extracted with 5% H_2O_2 (pH = 2) for 36 hr to selectively target the extraction of organic-bound Mo (Freslon et al., 2014). It is worth noting that prior to the above sequentially chemical extraction, we assessed the potential impact of exchangeable Mo on the Mo isotope composition of leached carbonate phases. To do so, selected powdered samples were washed with 1 M $MgCl_2$ (pH = 8) for 0.5 hr, as commonly used to extract exchangeable metals (Poulton & Canfield, 2005; Tessier et al., 1979) and further analyzed for elemental abundances. These experimental results indicate that exchangeable Mo systematically contributes to less than 20% (average of 12% ± 6%; 1 SD; $n = 9$; Table S1 in Supporting Information S1) relative to the amount of carbonate associated Mo extracted with our leaching procedure. Therefore, we are confident that the use of 5% acetic acid leaching of samples without preliminary removal of any exchangeable Mo still selectively targets carbonate-bound Mo.

All extractions were conducted on a mechanical shaker at room temperature. After each leaching step, the resulting residue obtained by centrifugation was thoroughly rinsed with deionized water (×4). After centrifugation, the supernatants were evaporated to dryness, and further digested by concentrated H_2O_2 and HNO_3 for hydroxylamine HCl, acetic acid, and H_2O_2 leachates. Finally, all processed leachates were re-dissolved in diluted 2% HNO_3 prior to analysis. Mo and other trace element abundances were determined by a Thermo Fisher X series 2 ICP-MS at Guizhou Tongwei Analytical Technology Co., Ltd. Certified reference materials (W-2a and BHVO-2) and a single standard solution of Mo were used for quality control with precision and accuracy both better than 5% for Fe, Mn, and Mo. Elemental abundances in the different separated phases of seep carbonate rocks are reported relative to the weight of bulk powdered samples.

2.2.5. Mo Isotope Compositions

The bulk-rock, total authigenic fraction, and carbonate and pyrite phases from seep carbonate rocks extracted by sequential leaching were analyzed for Mo isotopes at the State Key Laboratory of Isotope Geochemistry, Guangzhou Institute of Geochemistry, Chinese Academy of Science. Chemical separation was performed by ion chromatography using N-benzoyl-N-phenyl hydroxylamine (BPHA) resin and a mixed 6 M HF:1 M HCl solution for Mo elution following the procedures of Li et al. (2014). Chemical yields of Mo following separation were usually higher than 90%. The procedural blanks were less than 0.23 ng of Mo, contributing less than 1% of total Mo.

Molybdenum isotope measurements were performed on a Thermo-Fisher Scientific Neptune-Plus multi-collector inductively coupled plasma mass spectrometer (MC-ICP-MS) using the double-spike method (Li et al., 2014; Siebert et al., 2001). Prior to chemical separation, a ^{100}Mo-^{97}Mo double spike was added to samples for correction of instrumental mass bias and any other isotope fractionation occurring during chemical preparation. The NIST SRM 3134 Mo reference solution was repeatedly measured for monitoring the blank signal of the MC-ICP-MS.

Repeated measurements of a NIST SRM 3134 standard solution, USGS rock reference materials AGV-2, and IAPSO seawater standard yielded $\delta^{98}Mo$ values in relative to NIST SRM 3134 (0.25‰) of 0.25 ± 0.07‰ (2SD, $n = 26$), 0.08 ± 0.09‰ (2SD, $n = 4$), and 2.33 ± 0.02‰ (2SD, $n = 4$), respectively, in agreement with reference values (Greber et al., 2012; Li et al., 2014; P. Zhao et al., 2016). The analytical error of $\delta^{98}Mo$ values was less than 0.07‰ and typically less than 0.05‰ (2SD).

3. Results

3.1. Carbonate Minerals, $\delta^{13}C$, and $\delta^{18}O$ Compositions

The mineralogy of the studied samples is reported in Figure 2 and Table S2 in Supporting Information S1. Total carbonate contents vary between ca. 63 and 100 wt% (Table S2 in Supporting Information S1). Samples are dominated by LMC, aragonite, and HMC, with minor number of detrital minerals such as quartz, chlorite, and albite (Figure 2; Table S2 in Supporting Information S1). Based on carbonate mineralogy, the studied samples were classified into three categories: LMC, aragonite, and HMC, in which the dominant carbonate mineral phase accounted for more than 50% (Figure 2).

The $\delta^{13}C$ and $\delta^{18}O$ values of the carbonate fraction of seep carbonate rocks (i.e., $\delta^{13}C_{carb}$ and $\delta^{18}O_{carb}$) vary from −59.2‰ to −2.5‰ (Figure 3) and from 2.8 to 5.5‰ (Figure 3), respectively. For LMC- and aragonite-rich carbonates, $\delta^{13}C_{carb}$ values range from −51.7‰ to −23.9‰ and from −52.5‰ to −23.5‰, respectively (Figure 3). Note that the highest $\delta^{13}C_{carb}$ values in aragonite-rich samples are encountered in samples GC232 (−25.8‰) and AC645 (−23.5‰), while all other aragonite-rich samples display $\delta^{13}C_{carb}$ lower than −38.0‰ (Figure 3). The
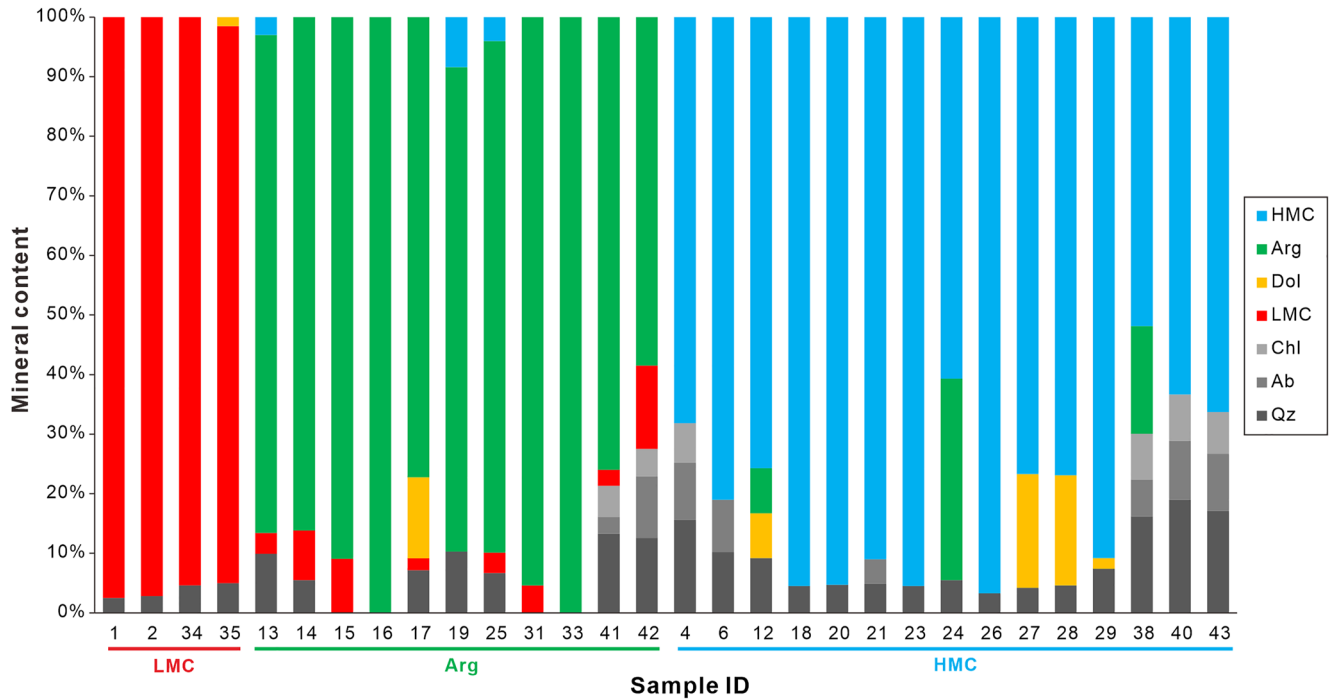
Figure 2. Mineral compositions of seep carbonate rocks. Minerals include high-magnesium calcite (HMC), aragonite (Arg), dolomite (Dol), low-magnesium calcite (LMC), chlorite (Chl), albite (Ab), and quartz (Qz). The studied samples can be categorized as carbonate dominated by LMC, Arg, or HMC. Samples 38 and 40–43 are carbonates from the South China Sea, while the other samples are carbonates from the Gulf of Mexico.

HMC-rich carbonates show two distinct ranges of $\delta^{13}C_{carb}$ values from −59.2‰ to −42.7‰ and from −21.9‰ to −2.5‰.

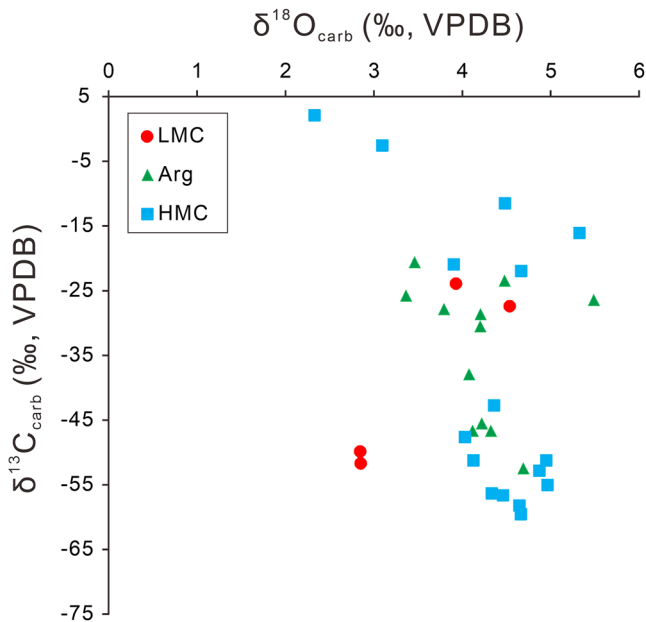**Figure 3.** $\delta^{13}C$ and $\delta^{18}O$ compositions of carbonate phases of the studied seep carbonate rocks. LMC, Arg, and high-magnesium calcite (HMC) refer to seep carbonate rocks that are dominated by low-magnesium calcite, aragonite, and HMC, respectively.

3.2. Element Contents

Carbonate samples exhibit an average TOC content of $2.34 \pm 2.73\%$ (1SD) ranging from 0.35% to 13.3% ($n = 23$), while S_{py} contents average $0.70 \pm 0.80\%$ (1SD) with a range from 0.02% to 3.04% ($n = 23$; Table S3 in Supporting Information S1; Figure 4). Samples 17–18 and 20–21 contain much higher TOC and S_{py}, varying from 1.45% to 13.3% and from 0.54% to 1.82%, respectively (Table S3 in Supporting Information S1), which reflect the influence of oil seepage on the chemistry of seep carbonate rocks at Site GC232 (Gulf of Mexico; Sun et al., 2020). HMC-rich carbonates exhibit the lowest TOC contents (0.35%–1.51%, mean 0.83%), compared to aragonite-rich (1.30%–5.71%, mean 2.46%), and LMC-rich carbonates (1.88%–5.79%, averaging 2.95%; Figure 4). Although S_{py} contents are more variable than TOC contents among different types of carbonates, the HMC-rich carbonates display the highest average content of S_{py} (1.22%; $n = 10$) compared to LMC (0.29%; $n = 4$) and aragonite (0.15%; $n = 6$; Figure 4; Table S3 in Supporting Information S1).

Authigenic Mn contents (Mn_{auth}) are lowest in aragonite-rich samples (6.6–218 μg/g, averaging 76 ± 58 μg/g, 1SD) (Figure 4; Table S3 in Supporting Information S1). Iron contents in total authigenic fractions (Fe_{auth}) display similar trends, being also lowest in aragonite samples (1,550–9,340 μg/g, averaging $4,775 \pm 2,525$ μg/g, 1SD). In the carbonate fractions, iron contents (Fe_{carb}) show no significant difference among different carbonate groups, with mean Fe_{carb} contents ranging between 1,468 and 1,530 μg/g. Iron contents in iron oxide fractions (Fe_{ox}) are similar in all types of samples. Consistent with the highest S_{py} contents in the HMC-rich carbonates, pyrite-bound Fe
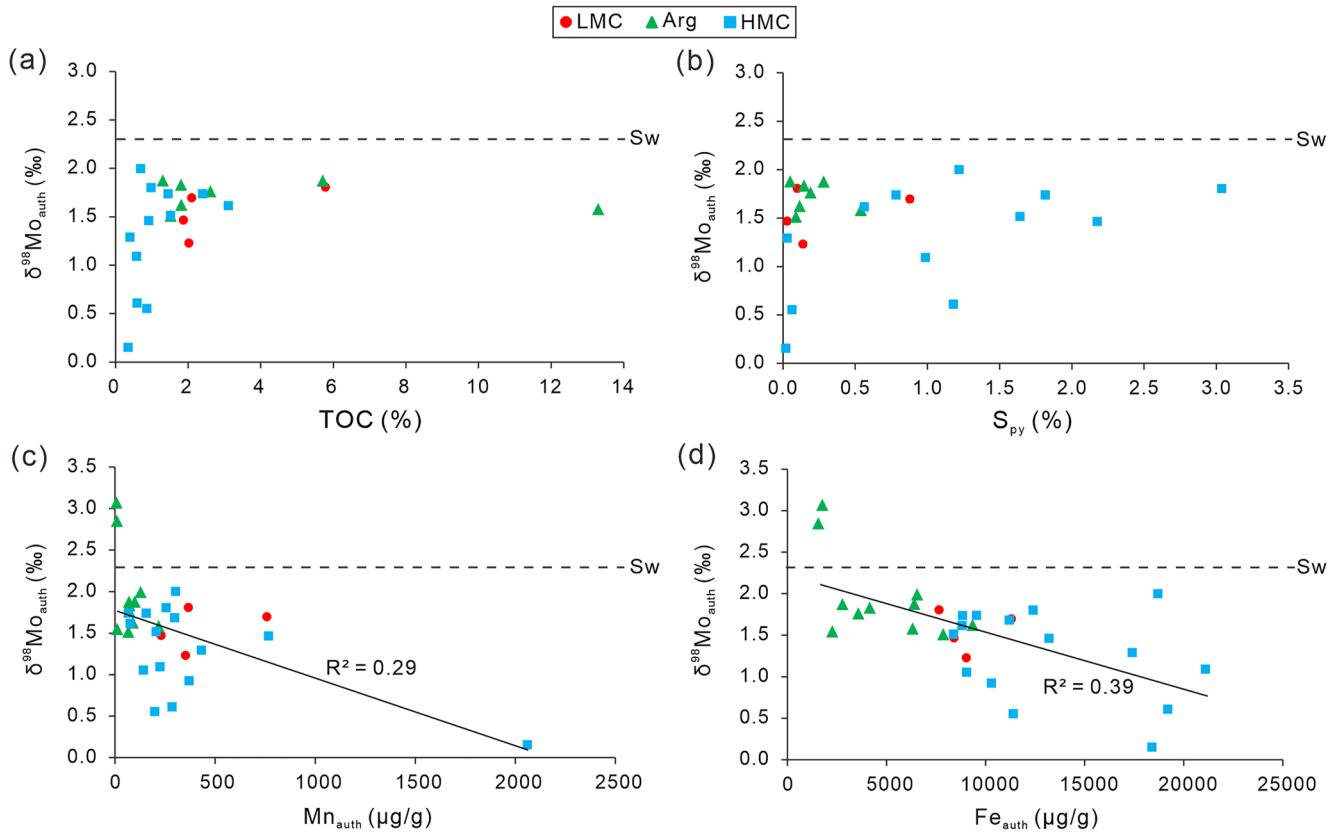
Figure 4. δ^{98}Mo values of authigenic Mo (δ^{98}Mo$_{auth}$) versus (a) contents of total organic carbon, (b) contents of pyrite sulfur (S_{py}), (c) manganese contents of total authigenic fraction (Mn$_{auth}$), and (d) iron contents of total authigenic fraction (Fe$_{auth}$) of seep carbonate rocks. LMC, Arg, and high-magnesium calcite (HMC) represent seep carbonate rocks that are dominated by low-magnesium calcite, aragonite, and HMC, respectively. The dashed line marks the seawater δ^{98}Mo value.

abundances (Fe$_{py}$) are also highest in HMC-rich samples, ranging from 4,110 to 13,000 µg/g. The contents of Fe (Fe$_{OM}$) bound to organic matter are uniformly low in all samples, ranging from 0.56 to 79.4 µg/g.

In terms of relative proportions, Fe$_{py}$ and Fe$_{carb}$ represent the dominant pools of total extracted Fe, accounting for average proportions of 55.4% and 29.9%, respectively (Figure S1 in Supporting Information S1), while Fe$_{ox}$ and Fe$_{OM}$ only account for approximately 14.3% and 0.4% of total extracted Fe, respectively (Figure S1 in Supporting Information S1). The extremely low Fe$_{OM}$ proportions less than 1.6% indicate that Fe$_{py}$ is close to completely extract during chemical extraction. Although XRD analysis did not identify pyrite in the studied samples, abundant pyrite was identified by microscopic and SEM observations (Feng & Chen, 2015; Huang et al., 2020; Roberts et al., 2010; see Figure S2 in Supporting Information S1).

Molybdenum contents of the total authigenic fractions (Mo$_{auth}$) are displayed in Figure 5. All aragonite-rich carbonates display Mo$_{auth}$ contents lower than 1.95 µg/g (Table S3 in Supporting Information S1). Relatively higher Mo$_{auth}$ contents were found for HMC carbonates ranging from 0.56 to 28.4 µg/g (mean: 8.5 µg/g; Figure 5; Table S3 in Supporting Information S1). Generally, Mo$_{auth}$ contents are in good agreement with the sum of all Mo fractions obtained by chemical extraction (Σ Mo; Figure 6a), which confirms the reliability of the applied sequential leaching protocol. Pyrite Mo (Mo$_{py}$) accounts for an average proportion of 70% in the studied seep carbonate rocks (Figure 6b). In some aragonite-rich samples, Mo abundance in carbonate fractions (Mo$_{carb}$) is higher than that in other phases (Figure 6b). In all studied samples, Mo from iron and manganese oxyhydroxide (Mo$_{ox}$) and organic matter (Mo$_{OM}$) represents only a minor fraction of the total Mo budget of seep carbonate rocks (Figure 6b).

3.3. δ^{98}Mo Compositions of Total Authigenic Fractions and Bulk-Rocks

The total authigenic fractions of seep carbonate rocks display δ^{98}Mo$_{auth}$ values between 0.15 and 3.07‰, averaging 1.56 ± 0.57‰ (1SD, n = 30; Table 2; Figures 4 and 5). δ^{98}Mo$_{auth}$ values are relatively higher in aragonite-rich

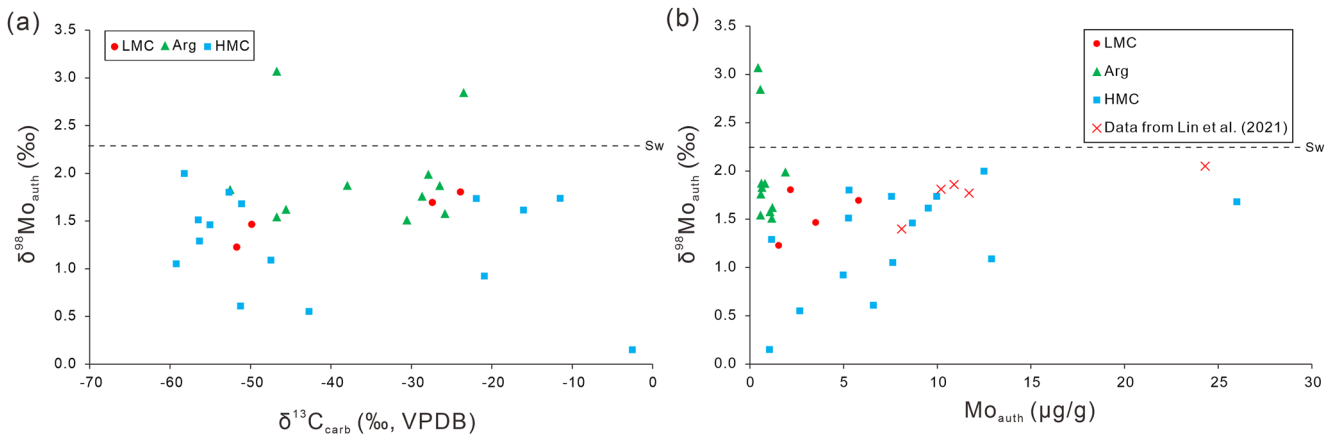**Figure 5.** $\delta^{98}Mo$ values of authigenic Mo ($\delta^{98}Mo_{auth}$) versus (a) $\delta^{13}C_{carb}$ values and (b) Mo_{auth} contents. $\delta^{13}C_{carb}$ represents $\delta^{13}C$ values of carbonate phases of seep carbonate rocks. LMC, Arg, and high-magnesium calcite (HMC) correspond to seep carbonate rocks that are dominated by low-magnesium calcite, aragonite, and HMC, respectively. The dashed line marks the seawater $\delta^{98}Mo$ value.

samples, varying from 1.51 to 3.07‰ with an average of 1.95 ± 0.50‰ (1SD, $n = 11$; Figure 5). For HMC and LMC carbonates, $\delta^{98}Mo_{auth}$ values range from 0.15 to 2.00‰ with an average of 1.34 ± 0.48‰ (1SD, $n = 19$; Figure 5; Table 2). In samples characterized by low TOC contents less than 1% and S_{py} contents less than 0.5%, $\delta^{98}Mo_{auth}$ values are highly variable (Figures 4a and 4b). In contrast, most samples characterized by higher TOC or S_{py} contents display high $\delta^{98}Mo_{auth}$ values (Figures 4a and 4b). To some extent, $\delta^{98}Mo_{auth}$ values increases with decreasing Mn_{auth} and Fe_{auth} contents (Figures 4c and 4d), while no apparent relationship is observed between $\delta^{98}Mo_{auth}$ and $\delta^{13}C_{carb}$ values (Figure 5a). $\delta^{98}Mo_{auth}$ values are highly variable in samples with Mo_{auth} contents of 2.5 µg/g or lower, but show less scatter when Mo_{auth} contents are higher (Figure 5b). Finally, the few $\delta^{98}Mo_{bulk}$ data are similar to $\delta^{98}Mo_{auth}$ values (Table 2; Figure S3 in Supporting Information S1 and Figure 7). Unlike findings from a previous study reporting similar $\delta^{98}Mo_{bulk}$ values in seep carbonate rocks with an average of 1.90‰ ($n = 5$; Lin et al., 2021), our results indicate a much larger variability of $\delta^{98}Mo_{bulk}$ and $\delta^{98}Mo_{auth}$ values, ranging from 1.02 to 1.98‰ (averaging 1.55 ± 0.35‰, 1SD, $n = 4$; Table 2) and 0.15–3.07‰ (averaging 1.56 ± 0.57‰, 1SD, $n = 30$; Table 2), respectively.

3.4. $\delta^{98}Mo$ Compositions of Sequentially Extracted Carbonate and Pyrite Phases

In general, $\delta^{98}Mo_{carb}$ values are the highest among all studied fractions, varying from 0.78 to 4.21‰ with an average of 2.02 ± 0.72‰ (1SD, $n = 15$; Table 2; Figure S3 in Supporting Information S1 and Figure 7). Values for $\delta^{98}Mo_{py}$ are generally lower than $\delta^{98}Mo_{carb}$, ranging from 0.00 to 2.09‰ with an average of 1.42 ± 0.72‰ (1SD, $n = 15$; Table 2). Nearly all $\delta^{98}Mo_{carb}$ are higher than $\delta^{98}Mo_{auth}$, except for samples 15 and 16 (Figure 7), which could reflect low Mo contents of these two samples. The plotted $\delta^{98}Mo_{py}$ and $\delta^{98}Mo_{auth}$ data approach a 1:1 linear relationship (Figure S3 in Supporting Information S1), which is consistent with the observation that Mo_{py} dominates the total Mo budget of seep carbonate rocks (Figure 6b). Compared with the aragonite-dominated carbonates, $\delta^{98}Mo_{carb}$ and $\delta^{98}Mo_{py}$ values of LMC and HMC carbonates exhibit less variability (Figure 7). The $\delta^{98}Mo_{carb}$ values of the LMC and HMC carbonates vary from 1.71 to 2.25‰ and 1.39–2.43‰, respectively (Table 2; Figure 7). The average $\delta^{98}Mo_{carb}$ values of LMC and HMC carbonates are close to the seawater $\delta^{98}Mo$ value of 2.3‰, yielding 1.98 ± 0.31‰ (1SD, $n = 10$). For the LMC and HMC carbonates, $\delta^{98}Mo_{py}$ values also exhibit less variability, ranging from 1.37 to 2.09‰ and 1.05–2.06‰, respectively (Figure 7). By contrast, $\delta^{98}Mo_{carb}$ and $\delta^{98}Mo_{py}$ values of aragonite carbonates display greater variations, from 0.78 to 4.21‰ and 0.00–1.86‰, respectively (Figure 7).

4. Discussion

4.1. Seep Carbonate Rocks Formed Under Variable Conditions

The mineralogy as well as the elemental and isotopic compositions of seep carbonate rocks provide information on fluid-sediment interactions and biogeochemical processes associated with carbonate precipitation (e.g.,
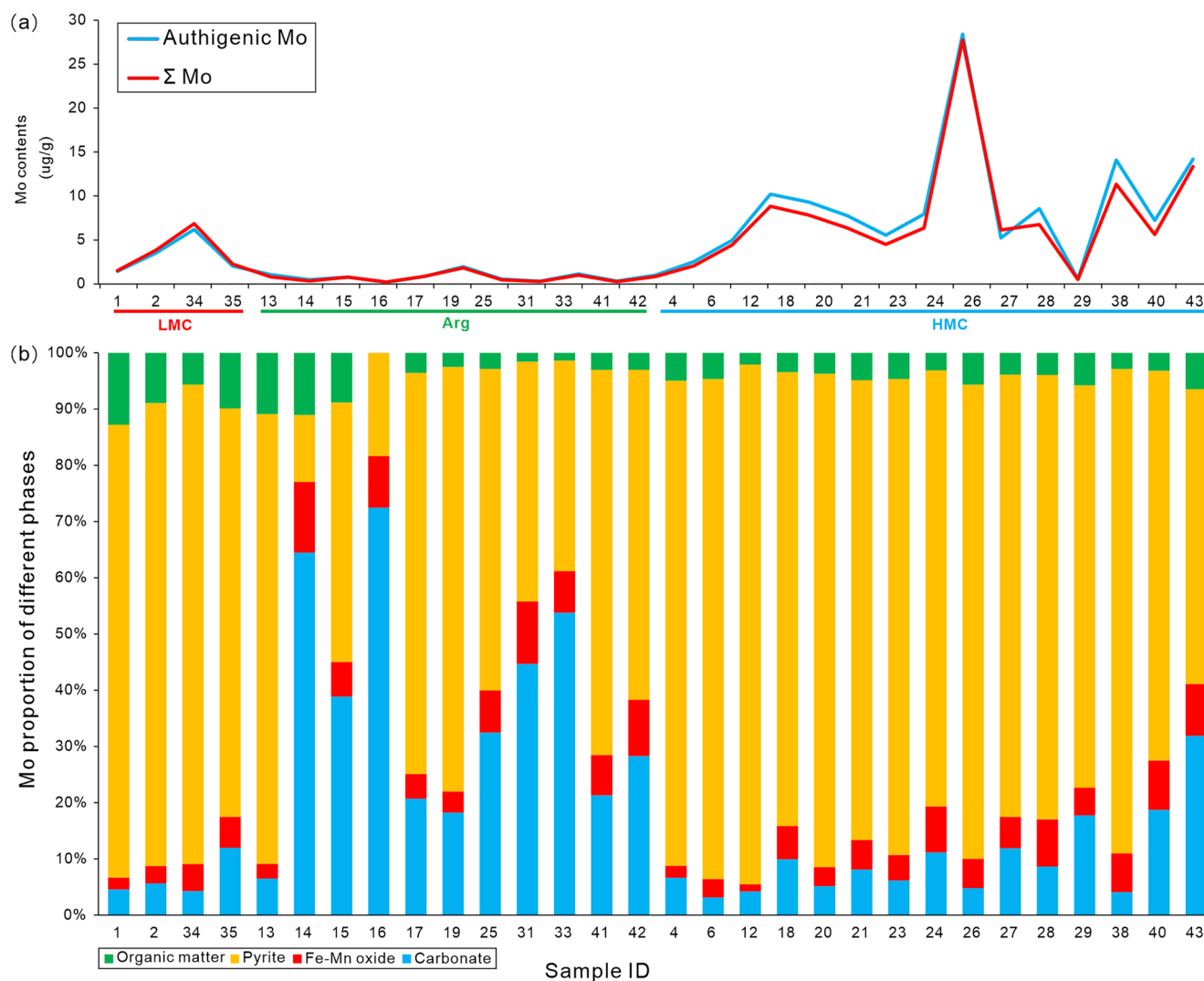
Figure 6. Molybdenum (Mo) contents and proportions of different phases for seep carbonate rocks. (a) Sum of Mo contents hosted in different phases by sequentially chemical extraction (Σ Mo) and authigenic Mo contents. (b) Relative proportions of Mo in different phases (i.e., carbonate, iron-manganese oxide, pyrite, and organic matter). The red, green, and blue lines mark seep carbonate rocks dominated by low-magnesium calcite (LMC), aragonite (Arg), and high-magnesium calcite.

Crémière, Lepland, Chand, Sahy, Condon, et al., 2016; Crémière, Lepland, Chand, Sahy, Kirsimäe, et al., 2016; Greinert et al., 2001; Hong et al., 2022; Hu et al., 2014; Liang et al., 2017; Naehr et al., 2007; Peckmann & Thiel, 2004; Pierre et al., 2015). For instance, the formation of aragonite is generally favored over HMC under near-seafloor conditions dominated by high sulfate contents, high Mg/Ca ratios and low H_2S concentrations in pore waters (e.g., Burton, 1993; Luff & Wallmann, 2003). Highly negative $\delta^{13}C_{carb}$ values ($<\delta^{13}C_{OM}$) are a diagnostic feature of AOM-driven carbonate precipitation near the SMT (e.g., Liang et al., 2017; Peckmann & Thiel, 2004). However, relatively high $\delta^{13}C_{carb}$ values, particularly when higher than local $\delta^{13}C_{OM}$ values, point toward either near-seafloor carbonate formation, reflecting a strong influence of relatively ^{13}C-enriched dissolved inorganic carbon from organoclastic sulfate reduction and the overlying bottom waters, or precipitation within the deeper methanogenic zone with ^{13}C-enriched fluids related to methanogenesis (e.g., Crémière, Lepland, Chand, Sahy, Kirsimäe, et al., 2016; Peckmann & Thiel, 2004; Pierre et al., 2015).

In this study, the higher $\delta^{13}C_{carb}$ values (from −27.9‰ to −25.8‰) measured in aragonite samples from site GC232 of the Gulf of Mexico are attributed to oil biodegradation near the seafloor (Tables 1 and 2; Sun et al., 2020). At site AC645, aragonite-rich samples display $\delta^{13}C_{carb}$ between −30.6‰ and −23.5‰, which, together with the presence of biomarkers of aerobic methanotrophic bacteria and negative cerium anomalies, are presumably indicative of carbonate precipitation under oxic to suboxic conditions (Table 2; Birgel et al., 2011;

Table 2
Carbon, Oxygen, and Molybdenum Isotope Values of Seep Carbonate Rocks

Sample ID	$\delta^{13}C_{carb}$ (‰)	$\delta^{18}O_{carb}$ (‰)	$\delta^{98}Mo_{auth}$ (‰)	$\delta^{98}Mo_{bulk}$ (‰)	$\delta^{98}Mo_{carb}$ (‰)	$\delta^{98}Mo_{py}$ (‰)
1	−51.7	2.9	1.23	n.d.	1.71	1.37
2	−49.8	2.8	1.47	1.46	1.96	1.52
4	−56.3	4.3	1.29	n.d.	n.d.	n.d.
6	−2.5	3.1	0.15	n.d.	n.d.	n.d.
12	−20.9	3.9	0.92	n.d.	n.d.	n.d.
13	−30.6	4.2	1.51	n.d.	n.d.	n.d.
14	−28.7	4.2	1.76	n.d.	n.d.	n.d.
15	−26.5	5.5	1.87	n.d.	1.74	1.51
16	−23.5	4.5	2.84	n.d.	0.78	0.00
17	−25.8	3.4	1.58	n.d.	n.d.	n.d.
18	−11.5	4.5	1.74	n.d.	1.98	1.59
19	−27.9	3.8	1.99	n.d.	n.d.	n.d.
20	−16.1	5.3	1.61	n.d.	n.d.	n.d.
21	−21.9	4.7	1.74	n.d.	n.d.	n.d.
23	−56.5	4.5	1.51	n.d.	n.d.	n.d.
24	−59.2	4.7	1.05	n.d.	1.39	1.05
25	−52.5	4.7	1.83	n.d.	2.26	1.86
26	−51.1	4.1	1.68	n.d.	n.d.	n.d.
27	−52.7	4.9	1.80	n.d.	2.35	1.94
28	−55.0	5.0	1.46	n.d.	1.93	1.57
29	−42.7	4.4	0.55	n.d.	n.d.	n.d.
31	−46.7	4.3	1.54	n.d.	n.d.	n.d.
33	−46.7	4.1	3.07	n.d.	4.21	0.00
34	−27.4	4.5	1.69	1.72	2.13	1.91
35	−23.9	3.9	1.80	n.d.	2.25	2.09
38	−47.4	4.0	1.09	1.02	1.69	1.07
40	−51.2	5.0	0.61	n.d.	n.d.	n.d.
41	−45.6	4.2	1.62	n.d.	1.51	1.70
42	−38.0	4.1	1.87	n.d.	n.d.	n.d.
43	−58.2	4.6	2.00	1.98	2.43	2.06

Note. $\delta^{13}C$ and $\delta^{18}O$ Values are Expressed Relative to the Vienna Pee Dee Belemnite Standard (V-PDB). $\delta^{98}Mo$ Values are Reported Relative to the NIST 3134 = +0.25‰ Standard. $\delta^{13}C_{carb}$ and $\delta^{18}O_{carb}$ represent $\delta^{13}C$ and $\delta^{18}O$ values of carbonate phase in the study seep carbonate rocks, respectively. $\delta^{98}Mo_{auth}$, $\delta^{98}Mo_{bulk}$, $\delta^{98}Mo_{carb}$, and $\delta^{98}Mo_{py}$ refer to Mo isotope values of total authigenic fraction, bulk-rock, carbonate, and pyrite of the seep carbonate rocks. n.d., no data.

Hu et al., 2014). For the other studied aragonite-rich samples, low $\delta^{13}C_{carb}$ values from −52.5‰ to −38.0‰ and low Mo_{auth} contents <1.2 µg/g imply that carbonates probably formed in the sulfate reduction zone, at relatively low pore water H_2S concentrations in relatively close vicinity to the seafloor (Figure 3; Table 2 and Table S2 in Supporting Information S1). For HMC-rich carbonates with either lower or higher $\delta^{13}C_{carb}$ values (Figure 3), high S_{py} and Fe_{py} contents agree with carbonate precipitation under strongly sulfidic conditions (Figures 3 and 4; Table 2 and Table S2 in Supporting Information S1). Similarly, LMC carbonates with relatively high contents of S_{py} and Fe_{py} most likely formed in a sulfidic environment (Hu et al., 2015; Figures 3 and 4).

4.2. $\delta^{98}Mo_{auth}$ Patterns During Early Diagenesis

Both experimental and field studies have provided evidence for the preferential adsorption of light Mo isotopes during iron and manganese oxide co-precipitation (e.g., Barling & Anbar, 2004; S. Chen et al., 2022; Eroglu et al., 2020; Goldberg et al., 2009; Scholz et al., 2017; Siebert et al., 2003; Wasylenki et al., 2008). Accordingly, Mo release related to the reduction of iron and manganese oxide phases in suboxic pore waters and subsequent precipitation of authigenic Mo is accompanied by a shift toward lower $\delta^{98}Mo$ values in both pore waters and Mo_{auth} relative to seawater (Eroglu et al., 2020; He et al., 2021; Hutchings et al., 2020; McManus et al., 2002; Scholz et al., 2017). In this study, the lowest $\delta^{98}Mo_{auth}$ values are generally encountered in seep carbonate rocks having the highest Fe_{auth} contents (Figure 4), hence consistent with the above-mentioned evidence that reduction of iron oxides yields low $\delta^{98}Mo$ signatures in pore waters from which seep carbonate rocks precipitate. Such low $\delta^{98}Mo_{auth}$ values, which are mostly encountered in HMC, probably reflect the influence of iron oxide reduction on the $\delta^{98}Mo_{auth}$ compositions during carbonate precipitation.

In addition to Mo sourced from the reduction of iron and manganese oxides, another potential source of dissolved Mo for Mo_{auth} is diffusive Mo supply from overlying bottom waters (Eroglu et al., 2020; Scholz et al., 2017). The LMC- and HMC-rich carbonates and some of the aragonite-rich carbonates, having formed under sulfidic conditions, exhibit both high Mo_{auth} and high $\delta^{98}Mo_{auth}$ compositions (Figure 5), consistent with previous observations (Lin et al., 2021). Due to the relatively low Mo contents in leached fractions of both iron and manganese oxyhydroxides and organic matter (Figure 6), the strong Mo_{auth} enrichment in these samples, which formed under sulfidic conditions, is possibly related to the input of Mo from seawater. Under sulfidic conditions, seawater-derived Mo is readily sequestered as Mo_{auth} during carbonate formation, and this process usually exerts no or some Mo isotope fractionation depending on ambient H_2S concentrations (e.g., Bura-Nakić et al., 2018; Gordon et al., 2009; Nägler et al., 2011; Neubert et al., 2008; Poulson et al., 2006; Romaniello et al., 2016). Critical H_2S concentrations of ∼11–100 µM have been considered as a threshold for Mo sequestration (e.g., Erickson & Helz, 2000; Helz et al., 1996, 2011; Zheng et al., 2000). At these threshold concentrations, a $\delta^{98}Mo$ offset of ∼0.5–0.7‰ would occur between Mo_{auth} and seawater Mo (Bura-Nakić et al., 2018). In contrast, no Mo isotope fractionation is thought to occur above this critical H_2S concentration with nearly quantitative Mo removal (e.g., Bura-Nakić et al., 2018; Gordon et al., 2009; Hutchings et al., 2020; Nägler et al., 2011; Neubert et al., 2008; Poulson et al., 2006; Romaniello et al., 2016). The above relationships between Mo isotope fractionation and dissolved H_2S concentration in the pore waters most likely account for the observed higher $\delta^{98}Mo_{auth}$ values, with an average offset of 0.7‰ relative to seawater in the LMC and HMC carbonates (Figure 4). In contrast, the fact that those samples with $\delta^{98}Mo_{auth}$ lower than seawater values (with offsets exceeding 0.7‰)
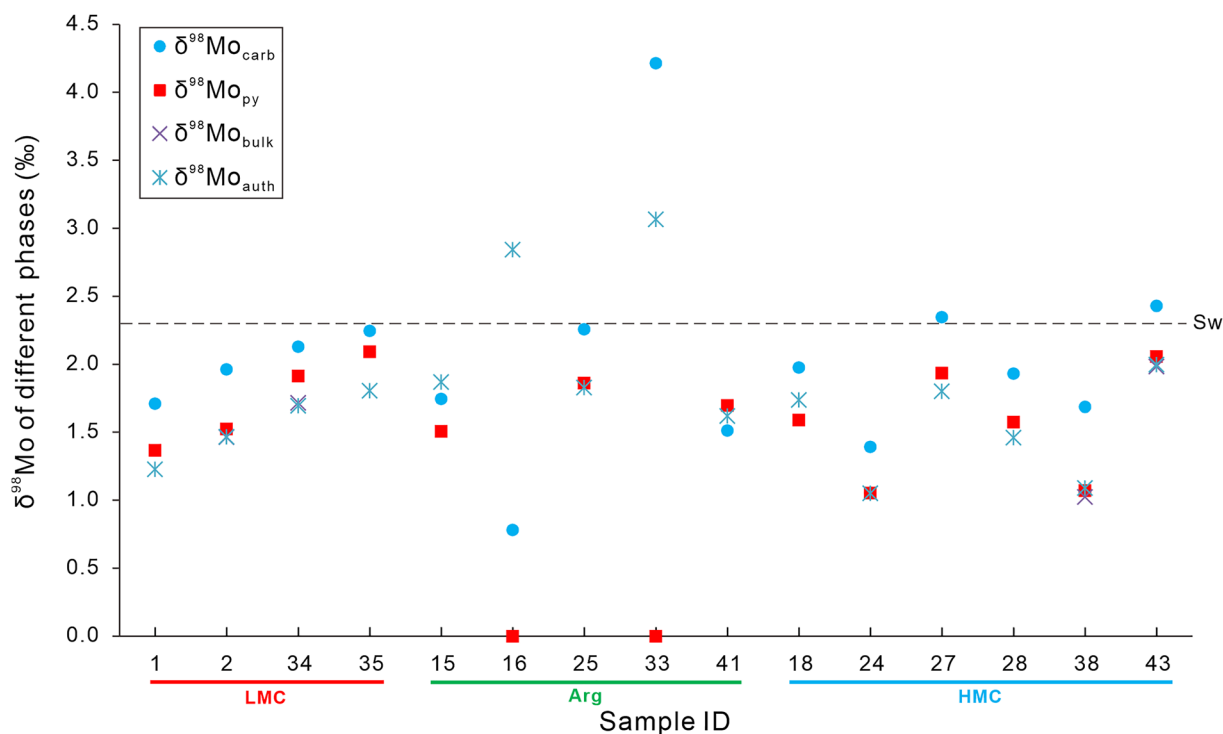
Figure 7. δ^{98}Mo values of different phases of samples, including carbonate (δ^{98}Mo$_{carb}$), pyrite (δ^{98}Mo$_{py}$), bulk-rock (δ^{98}Mo$_{bulk}$), and authigenic phase (δ^{98}Mo$_{auth}$). The red, green, and blue lines mark seep carbonate rocks dominated by low-magnesium calcite (LMC), aragonite (Arg), and high-magnesium calcite. The dashed line marks the seawater δ^{98}Mo value.

also formed in sulfidic environments (Figure 4) probably reflects the superimposed influence of lower δ^{98}Mo signatures derived from iron and manganese oxide reduction. Alternatively, such low δ^{98}Mo$_{auth}$ values can possibly result from a large isotopic fractionation between seawater molybdate and thiomolybdate species at low H$_2$S concentrations (<10 μM; Azrieli-Tal et al., 2014; He et al., 2021).

For those aragonite samples (ID 14–16) that apparently formed under oxic to suboxic conditions, Mo$_{auth}$ is mostly derived from carbonate-bound Mo (Mo$_{carb}$; Figure 6). For samples 15 and 16, the observed higher δ^{98}Mo$_{auth}$ values relative to both δ^{98}Mo$_{py}$ and δ^{98}Mo$_{carb}$ compositions could result from an underestimation of δ^{98}Mo$_{py}$ and δ^{98}Mo$_{carb}$ or an overestimation of δ^{98}Mo$_{auth}$ values induced using our sample leaching procedure. With respect to seep carbonate rocks forming near the seafloor, Mo$_{auth}$ can be sourced from bottom waters, iron and manganese oxyhydroxide phases, and organic matter remineralization. Recent experimental observations have suggested that calcite precipitation itself is probably accompanied by only limited Mo isotopic fractionation (X. Chen et al., 2021), implying that the δ^{98}Mo$_{carb}$ faithfully preserve the δ^{98}Mo signature of the pore fluids from which seep carbonate rocks precipitate. Since the release of dissolved Mo from iron and manganese oxyhydroxide phases probably results in a shift toward lighter δ^{98}Mo compositions of pore waters (Eroglu et al., 2020; He et al., 2021; Hutchings et al., 2020; McManus et al., 2002; Scholz et al., 2017), iron and manganese reduction could account for δ^{98}Mo$_{auth}$ values in aragonite-rich samples lower than the seawater value. In contrast, much higher pore water δ^{98}Mo values relative to seawater have been observed at greater sediment depths in the suboxic to anoxic zones below the seafloor along ocean margins, reflecting preferential adsorption of light Mo by iron and manganese oxides and, as a consequence, a shift toward heavier Mo isotope signatures of pore waters (Hutchings et al., 2020; McManus et al., 2002). By inference, precipitation of seep carbonate rocks from such isotopically heavy pore waters can possibly explain some of the high δ^{98}Mo$_{auth}$ values (as high as 3.07‰) observed in this study whenever the carbonate mineral phases dominate the authigenic Mo pool.

4.3. Implications of δ98Mo Distribution Patterns in Carbonate and Pyrite Phases During Early Diagenesis

The observation that Mo$_{auth}$ contents generally agree with the sum of the different Mo fractions obtained by chemical extraction provides reassuring evidence for the reliability of the applied sequential leaching protocol and the

near complete extraction of Mo during leaching (Figure 6a). Although no synthetic standard was used in this study to monitor any potential Mo isotope fractionation during sequential leaching, the near complete extraction of authigenic Mo fractions suggests that isotope fractionation was probably negligible. This inference is consistent with the results that pyrite dominates the Mo budget and $\delta^{98}Mo$ signature of seep carbonate rocks (Figure 6 and Figure S3 in Supporting Information S1). The preferential adsorption of isotopically light Mo onto iron and manganese oxides upon co-precipitation can result in a shift toward an isotopically heavier Mo isotope signature in ambient pore waters (Hutchings et al., 2020; McManus et al., 2002). Under such circumstances, aragonite precipitating from pore waters would incorporate isotopically heavy Mo of pore water, which explains the higher $\delta^{98}Mo_{carb}$ values relative to the seawater $\delta^{98}Mo$ value observed in aragonite-rich samples (Figure 7). Alternatively, the high $\delta^{98}Mo_{carb}$ values in aragonite-rich samples could also result from large Mo isotope fractionation at low H_2S concentrations ($<10\ \mu M$) and high Mo concentrations (Azrieli-Tal et al., 2014), yielding residual ^{98}Mo enriched pore waters. A peculiarity of our data set is the occurrence of particularly low $\delta^{98}Mo_{py}$ values (ca. 0‰) in a few aragonite samples (Figure 7). We attribute this feature to the highly dynamic nature of fluid seepage and associated redox conditions within microenvironments at seeps (e.g., Solomon et al., 2008; Tryon et al., 1999), favoring late precipitation of sulfide minerals at a microscale within aragonite-rich deposits. In such cases, such later-stage sulfides will presumably inherit the relatively low $\delta^{98}Mo$ composition of initial iron and manganese oxyhydroxides that were reduced and further interacted with ambient H_2S to form pyrite, hence resulting in the observed near-zero $\delta^{98}Mo_{py}$ signatures.

As mentioned above, the exchangeable Mo fraction is minor relative to the total Mo budget of carbonates (Table S1 in Supporting Information S1). This pool mostly corresponds to Mo that exchanged between dissolved pore waters and solid-phase. Therefore, the isotopic signatures of exchangeable Mo and dissolved Mo (i.e., pore water Mo) should be similar. Because $\delta^{98}Mo_{carb}$ values have been demonstrated to faithfully reflect the $\delta^{98}Mo$ composition of pore waters from which authigenic carbonates have precipitated (X. Chen et al., 2021), the obtained $\delta^{98}Mo_{carb}$ values represent the $\delta^{98}Mo$ composition of the dissolved Mo pool in the pore water from which carbonates precipitated. Consequently, the degree of Mo isotope fractionation during the incorporation of dissolved Mo into Mo_{auth} can be estimated from the difference between $\delta^{98}Mo_{carb}$ and $\delta^{98}Mo_{py}$. Upon the intense sulfate reduction, seep environments are typically characterized by high H_2S concentrations on the mM scale with a steep gradient of H_2S concentrations (e.g., Aharon & Fu, 2000; Joye, 2020; Joye et al., 2010; Niewöhner et al., 1998). Excess H_2S concentrations above the $\sim11–100\ \mu M$ threshold result in quantitative removal of dissolved Mo from pore waters with negligible Mo isotope fractionation (Bura-Nakić et al., 2018; Nägler et al., 2011; Romaniello et al., 2016). Such a scenario is expected to result in lower Mo fractionation between $\delta^{98}Mo_{carb}$ and $\delta^{98}Mo_{py}$ ($\Delta^{98}Mo_{carb-py}$) with higher Mo_{auth} and Mo_{py} contents. However, this hypothesis is not supported by our data, which actually show that lower $\Delta^{98}Mo_{carb-py}$ correlates with low Mo_{auth} and Mo_{py} contents in the LMC and HMC carbonates (Figure 8). The new data rather suggest that most Mo_{auth} sequestration takes place at a critical H_2S concentration, coming along with Mo isotope fractionation (Figure 8). This conclusion is consistent with the observation that Mo isotopes can fractionate during high Mo uptake in carbonate-rich marine sediments at critical H_2S concentrations (Bura-Nakić et al., 2020). Under such circumstances, $\delta^{98}Mo_{auth}$ and $\delta^{98}Mo_{py}$ values are lower than $\delta^{98}Mo$ composition of seawater; however, $\delta^{98}Mo_{carb}$ values as an archive of pore water isotope composition of Mo should be slightly higher or approach the $\delta^{98}Mo$ composition of seawater. This conclusion is supported by the observation that $\delta^{98}Mo_{carb}$ signatures with an average of $1.98 \pm 0.31‰$ (1 SD; $n = 10$) formed under sulfidic conditions at seeps are closer to the seawater value compared with $\delta^{98}Mo_{bulk}$, $\delta^{98}Mo_{auth}$, and $\delta^{98}Mo_{py}$ compositions (Figure 7; Table 2).

Non-skeletal carbonates, in particular authigenic Mo in carbonate-dominated sediments or seep carbonate rocks reflecting sulfidic pore water conditions have been proposed as reliable archives recording the $\delta^{98}Mo$ composition of past seawater (Bura-Nakić et al., 2020; Clarkson et al., 2020; Czaja et al., 2012; Lin et al., 2021; Romaniello et al., 2016; Voegelin et al., 2009, 2010). However, the applicability of authigenic Mo as an archive for seawater $\delta^{98}Mo$ appears to be complicated for carbonates, given the large variability of $\delta^{98}Mo_{bulk}$ and $\delta^{98}Mo_{auth}$ observed in this study, which commonly exhibit values significantly lower than seawater (Figure 7). In contrast, seep carbonate rocks forming under sulfidic conditions display a relatively narrower range of $\delta^{98}Mo_{carb}$ values (Figure 7). We therefore propose here that the $\delta^{98}Mo_{carb}$ of seep carbonate rocks could provide constraints on ancient seawater $\delta^{98}Mo$ signatures. Additionally, the highly variable $\delta^{98}Mo$ signature of different phases recorded in aragonite-rich seep carbonate rocks could be useful to trace the highly dynamic nature of fluid seepage and the complex local biogeochemical processes. The formation of authigenic carbonate in marine sediments possibly played a major
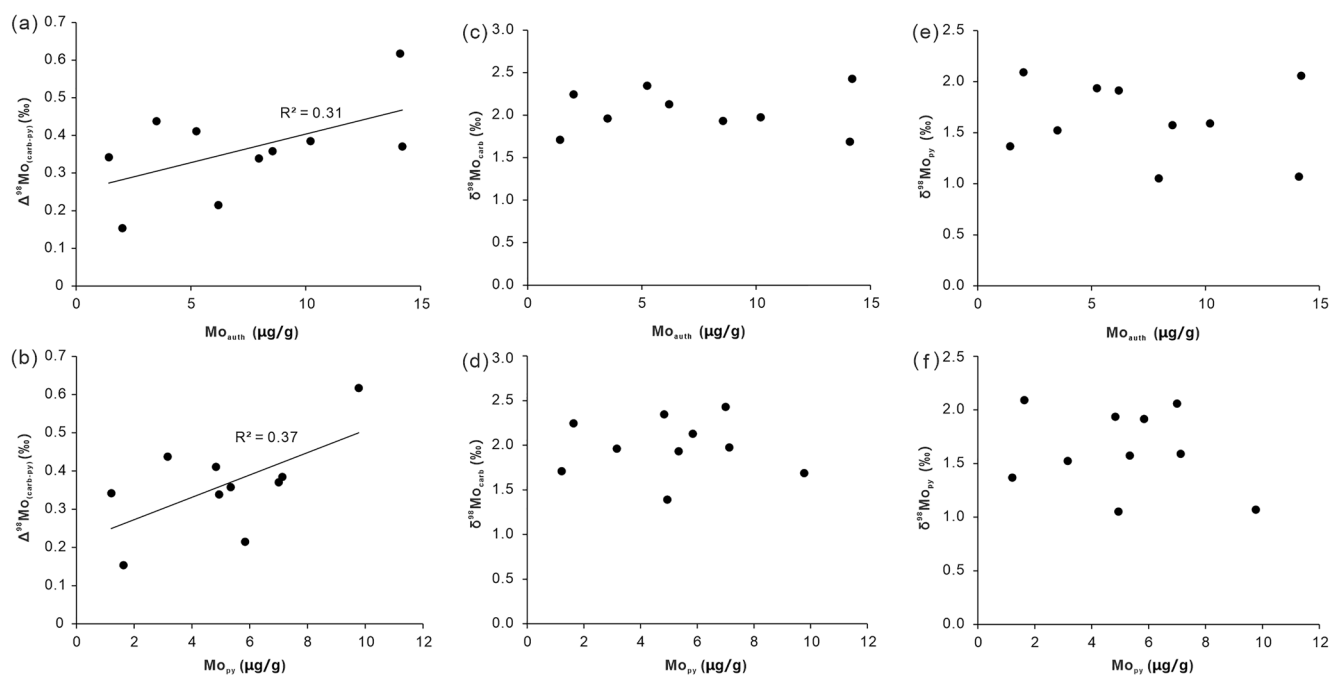
Figure 8. Plots of Mo isotopes and Mo contents of seep carbonate rocks. (a) Difference in $\delta^{98}Mo$ between carbonate and pyrite phases ($\Delta^{98}Mo_{(carb-py)}$) versus contents of authigenic Mo (Mo_{auth}). (b) $\Delta^{98}Mo_{(carb-py)}$ versus Mo contents of pyrite in the seep carbonate rocks (Mo_{py}). (c) $\delta^{98}Mo_{carb}$ versus Mo_{auth}. (d) $\delta^{98}Mo_{carb}$ versus Mo_{py}. (e) $\delta^{98}Mo_{py}$ versus Mo_{auth}. (f) $\delta^{98}Mo_{py}$ versus Mo_{py}.

role in the global carbon cycle over geological timescales (Schrag et al., 2013; Wang et al., 2023). Distinguishing between authigenic carbonates and primary marine carbonates in the geological record is thus fundamental to understanding the long-term carbon cycle and its role in regulating the evolution of atmospheric oxygen throughout Earth's history (M. Y. Zhao et al., 2016). The observed offsets between $\delta^{98}Mo_{carb}$ and seawater $\delta^{98}Mo$ in the studied authigenic carbonate rocks probably resulted from the capture of isotopically light dissolved Mo, which was released during the reduction of abundant iron and manganese oxides, into the carbonate phase during carbonate formation in sediments. Such $\delta^{98}Mo$ offsets may not be present in primary marine carbonates that form in the open-ocean water column due to the presumably reduced influence of authigenic iron and manganese oxides (Voegelin et al., 2009, 2010). Therefore, in addition to more conventional proxies such as U abundances and stable carbon isotopes (M. Y. Zhao et al., 2016), the $\delta^{98}Mo$ composition of different extractable fractions of sedimentary carbonate rocks can possibly serve as a new proxy for distinguishing between primary and authigenic carbonates in the geological record.

5. Conclusions

Authigenic carbonates from various seeps of the Gulf of Mexico and the South China Sea were used to investigate the behavior of Mo isotopes during early diagenesis. Results from a sequential leaching procedure targeting (a) carbonate, (b) iron and manganese oxides, (c) pyrite, and (d) organic phases of seep carbonate rocks, in addition to bulk-rock and total authigenic fractions, indicate that pyrite dominates the Mo budget and the $\delta^{98}Mo$ signature of seep carbonate rocks. It is found that the difference in $\delta^{98}Mo$ values between carbonate and pyrite fractions of seep carbonate rocks increases with increasing Mo contents, which we interpret as reflecting the critical control of hydrogen sulfide (H_2S) concentrations on $\delta^{98}Mo$ distribution patterns in sulfidic environments. The sequestration of authigenic Mo under weakly sulfidic conditions is associated with Mo isotope fractionation, resulting in relatively low $\delta^{98}Mo$ values in extracted pyrite fractions compared to seawater. However, the $\delta^{98}Mo$ composition of leached carbonate phases (mean: 1.98 ± 0.31‰, 1SD; $n = 10$) extracted from samples formed under sulfidic conditions is closer to the seawater value compared to the other leached phases. This observation suggests that the $\delta^{98}Mo$ composition of the carbonate fraction of seep carbonate rocks can provide useful constraints on ancient seawater $\delta^{98}Mo$ signatures. Overall, these findings show that Mo isotope systematics of sequentially extracted phases of seep carbonate rocks could serve as a new tool for investigating past biogeochemical processes and improving paleoenvironmental reconstructions.

Conflict of Interest

The authors declare no conflicts of interest relevant to this study.

Data Availability Statement

All the data used in the study have been included in the tables of the main text and Supporting Information S1. Additionally, these data are also included in the Mendeley Data Repository (Jia et al., 2023).

References

Aharon, P., & Fu, B. (2000). Microbial sulfate reduction rates and sulfur and oxygen isotope fractionations at oil and gas seeps in deepwater Gulf of Mexico. *Geochimica et Cosmochimica Acta*, *64*(2), 233–246. https://doi.org/10.1016/S0016-7037(99)00292-6

Arnold, G. L., Anbar, A. D., Barling, J., & Lyons, T. W. (2004). Molybdenum isotope evidence for widespread anoxia in mid-Proterozoic oceans. *Science*, *304*(5667), 87–90. https://doi.org/10.1126/science.1091785

Azrieli-Tal, I., Matthews, A., Bar-Matthews, M., Almogi-Labin, A., Vance, D., Archer, C., & Teutsch, N. (2014). Evidence from molybdenum and iron isotopes and molybdenum–uranium covariation for sulphidic bottom waters during Eastern Mediterranean sapropel S1 formation. *Earth and Planetary Science Letters*, *393*, 231–242. https://doi.org/10.1016/j.epsl.2014.02.054

Barling, J., & Anbar, A. D. (2004). Molybdenum isotope fractionation during adsorption by manganese oxides. *Earth and Planetary Science Letters*, *217*(3–4), 315–329. https://doi.org/10.1016/S0012-821X(03)00608-3

Barling, J., Arnold, G. L., & Anbar, A. D. (2001). Natural mass dependent variations in the isotopic composition of molybdenum. *Earth and Planetary Science Letters*, *193*(3–4), 447–457. https://doi.org/10.1016/S0012-821X(01)00514-3

Birgel, D., Feng, D., Roberts, H. H., & Peckmann, J. (2011). Changing redox conditions at cold seeps as revealed by authigenic carbonates from Alaminos Canyon, northern Gulf of Mexico. *Chemical Geology*, *285*(1–4), 82–96. https://doi.org/10.1016/j.chemgeo.2011.03.004

Boetius, A., Ravenschlag, K., Schubert, C. J., Rickert, D., Widdel, F., Gieseke, A., et al. (2000). A marine microbial consortium apparently mediating anaerobic oxidation of methane. *Nature*, *407*(6804), 623–626. https://doi.org/10.1038/35036572

Bura-Nakić, E., Andersen, M. B., Archer, C., De Souza, G. F., Marguš, M., & Vance, D. (2018). Coupled Mo-U abundances and isotopes in a small marine euxinic basin: Constraints on processes in euxinic basins. *Geochimica et Cosmochimica Acta*, *222*, 212–229. https://doi.org/10.1016/j.gca.2017.10.023

Bura-Nakić, E., Sondi, I., Mikac, N., & Andersen, M. B. (2020). Investigating the molybdenum and uranium redox proxies in a modern shallow anoxic carbonate rich marine sediment setting of the Malo Jezero (Mljet Lakes, Adriatic Sea). *Chemical Geology*, *533*, 119441. https://doi.org/10.1016/j.chemgeo.2019.119441

Burton, E. A. (1993). Controls on marine carbonate cement mineralogy: Review and reassessment. *Chemical Geology*, *105*(1–3), 163–179. https://doi.org/10.1016/0009-2541(93)90124-2

Burton, E. A., & Walter, L. M. (1991). The effects of PCO_2 and temperature on magnesium incorporation in calcite in seawater and $MgCl_2$-$CaCl_2$ solutions. *Geochimica et Cosmochimica Acta*, *55*(3), 777–785. https://doi.org/10.1016/0016-7037(91)90341-2

Chao, T., & Sanzolone, R. F. (1977). Chemical dissolution of sulfide minerals. *Journal Research of the U.S. Geological Survey*, *5*, 409–412.

Chen, F., Hu, Y., Feng, D., Zhang, X., Cheng, S., Gao, J., et al. (2016). Evidence of intense methane seepages from molybdenum enrichments in gas hydrate-bearing sediments of the northern South China Sea. *Chemical Geology*, *443*, 173–181. https://doi.org/10.1016/j.chemgeo.2016.09.029

Chen, S., Peng, X., Li, J., Lin, Z., Li, H., Wei, G., et al. (2022). Extremely light molybdenum isotope signature of sediments in the Mariana Trench. *Chemical Geology*, *605*, 120959. https://doi.org/10.1016/j.chemgeo.2022.120959

Chen, X., Ling, H. F., Vance, D., Shields-Zhou, G. A., Zhu, M., Poulton, S. W., et al. (2015). Rise to modern levels of ocean oxygenation coincided with the Cambrian radiation of animals. *Nature Communications*, *6*(1), 7142. https://doi.org/10.1038/ncomms8142

Chen, X., Romaniello, S. J., & Anbar, A. D. (2021). Preliminary exploration of molybdenum isotope fractionation during coprecipitation of molybdate with abiotic and microbial calcite. *Chemical Geology*, *566*, 120102. https://doi.org/10.1016/j.chemgeo.2021.120102

Cheng, M., Li, C., Jin, C., Wang, H., Algeo, T. J., Lyons, T. W., et al. (2020). Evidence for high organic carbon export to the early Cambrian seafloor. *Geochimica et Cosmochimica Acta*, *287*, 125–140. https://doi.org/10.1016/j.gca.2020.01.050

Clarkson, M. O., Müsing, K., Andersen, M. B., & Vance, D. (2020). Examining pelagic carbonate-rich sediments as an archive for authigenic uranium and molybdenum isotopes using reductive cleaning and leaching experiments. *Chemical Geology*, *539*, 119412. https://doi.org/10.1016/j.chemgeo.2019.119412

Colodner, D., Edmond, J., & Boyle, E. (1995). Rhenium in the Black Sea: Comparison with molybdenum and uranium. *Earth and Planetary Science Letters*, *131*(1–2), 1–15. https://doi.org/10.1016/0012-821X(95)00010-A

Crémière, A., Lepland, A., Chand, S., Sahy, D., Condon, D. J., Noble, S. R., et al. (2016). Timescales of methane seepage on the Norwegian margin following collapse of the Scandinavian Ice Sheet. *Nature Communications*, *7*(1), 11509. https://doi.org/10.1038/ncomms11509

Crémière, A., Lepland, A., Chand, S., Sahy, D., Kirsimäe, K., Bau, M., et al. (2016). Fluid source and methane-related diagenetic processes recorded in cold seep carbonates from the Alvheim channel, central North Sea. *Chemical Geology*, *432*, 16–33. https://doi.org/10.1016/j.chemgeo.2016.03.019

Czaja, A. D., Johnson, C. M., Roden, E. E., Beard, B. L., Voegelin, A. R., Nägler, T. F., et al. (2012). Evidence for free oxygen in the Neoarchean ocean based on coupled iron-molybdenum isotope fractionation. *Geochimica et Cosmochimica Acta*, *86*, 118–137. https://doi.org/10.1016/j.gca.2012.03.007

Deng, Y., Chen, F., Hu, Y., Guo, Q., Cao, J., Chen, H., et al. (2020). Methane seepage patterns during the middle Pleistocene inferred from molybdenum enrichments of seep carbonates in the South China Sea. *Ore Geology Reviews*, *125*, 103701. https://doi.org/10.1016/j.oregeorev.2020.103701

Dickson, A. J., Cohen, A. S., & Coe, A. L. (2014). Continental margin molybdenum isotope signatures from the early Eocene. *Earth and Planetary Science Letters*, *404*, 389–395. https://doi.org/10.1016/j.epsl.2014.08.004

Emerson, S. R., & Huested, S. S. (1991). Ocean anoxia and the concentrations of molybdenum and vanadium in seawater. *Marine Chemistry*, *34*(3–4), 177–196. https://doi.org/10.1016/0304-4203(91)90002-E

Erickson, B. E., & Helz, G. R. (2000). Molybdenum (VI) speciation in sulfidic waters: Stability and lability of thiomolybdates. *Geochimica et Cosmochimica Acta*, *64*(7), 1149–1158. https://doi.org/10.1016/S0016-7037(99)00423-8

Eroglu, S., Scholz, F., Frank, M., & Siebert, C. (2020). Influence of particulate versus diffusive molybdenum supply mechanisms on the molybdenum isotope composition of continental margin sediments. *Geochimica et Cosmochimica Acta*, *273*, 51–69. https://doi.org/10.1016/j.gca.2020.01.009

Feng, D., & Chen, D. (2015). Authigenic carbonates from an active cold seep of the northern South China Sea: New insights into fluid sources and past seepage activity. *Deep-Sea Research II: Topical Studies in Oceanography*, *122*, 74–83. https://doi.org/10.1016/j.dsr2.2015.02.003

Freslon, N., Bayon, G., Toucanne, S., Bermell, S., Bollinger, C., Chéron, S., et al. (2014). Rare earth elements and neodymium isotopes in sedimentary organic matter. *Geochimica et Cosmochimica Acta*, *140*, 177–198. https://doi.org/10.1016/j.gca.2014.05.016

Goldberg, T., Archer, C., Vance, D., & Poulton, S. W. (2009). Mo isotope fractionation during adsorption to Fe (oxyhydr)oxides. *Geochimica et Cosmochimica Acta*, *73*(21), 6502–6516. https://doi.org/10.1016/j.gca.2009.08.004

Goldberg, T., Archer, C., Vance, D., Thamdrup, B., McAnena, A., & Poulton, S. W. (2012). Controls on Mo isotope fractionations in a Mn-rich anoxic marine sediment, Gullmar Fjord, Sweden. *Chemical Geology*, *296–297*, 73–82. https://doi.org/10.1016/j.chemgeo.2011.12.020

Goldberg, T., Poulton, S. W., Wagner, T., Kolonic, S. F., & Rehkämper, M. (2016). Molybdenum drawdown during Cretaceous Oceanic Anoxic Event 2. *Earth and Planetary Science Letters*, *440*, 81–91. https://doi.org/10.1016/j.epsl.2016.02.006

Goldsmith, J. R., Graf, D. L., & Heard, H. C. (1961). Lattice constants of the calcium-magnesium carbonates. *Amercian Mineralogist*, *46*, 453–457.

Gordon, G. W., Lyons, T. W., Arnold, G. L., Roe, J., Sageman, B. B., & Anbar, A. D. (2009). When do black shales tell molybdenum isotope tales? *Geology*, *37*(6), 535–538. https://doi.org/10.1130/G25186A.1

Greber, N. D., Siebert, C., Nägler, T. F., & Pettke, T. (2012). $\delta^{98/95}$Mo values and molybdenum concentration data for NIST SRM 610, 612 and 3134: Towards a common protocol for reporting Mo data. *Geostands and Geoanalytical Research*, *36*(3), 291–300. https://doi.org/10.1111/j.1751-908X.2014.12047.x

Greinert, J., Bohrmann, G., & Suess, E. (2001). Gas hydrate-associated carbonates and methane-venting at hydrate ridge: Classification, distribution and origin of authigenic lithologies. In C. K. Paull & W. P. &Dillon (Eds.), *Natural Gas Hydrates: Occurrence, Distribution, and Detection, Geophysical Monographs* (Vol. 124, pp. 99–113). American Geophysical Union.

Guan, H., Liu, L., Hu, Y., Li, S. Z., Li, N., Sun, Z., et al. (2022). Rising bottom-water temperatures induced methane release during the middle Holocene in the Okinawa Trough, East China Sea. *Chemical Geology*, *590*, 120707. https://doi.org/10.1016/j.chemgeo.2022.120707

Han, Y. M., Cao, J., Posmentier, E. S., Chow, J. C., Watson, J. G., Fung, K. K., et al. (2009). The effect of acidification on the determination of elemental carbon, char-and soot-elemental carbon in soils and sediments. *Chemosphere*, *75*(1), 92–99. https://doi.org/10.1016/j.chemosphere.2008.11.044

He, Z., Clarkson, M. O., Andersen, M. B., Archer, C., Sweere, T. C., Kraal, P., et al. (2021). Temporally and spatially dynamic redox conditions on an upwelling margin: The impact on coupled sedimentary Mo and U isotope systematics, and implications for the Mo-U paleoredox proxy. *Geochimica et Cosmochimica Acta*, *309*, 251–271. https://doi.org/10.1016/j.gca.2021.06.024

Helz, G. R., Bura-Nakić, E., Mikac, N., & Ciglenečki, I. (2011). New model for molybdenum behavior in euxinic waters. *Chemical Geology*, *284*(3–4), 323–332. https://doi.org/10.1016/j.chemgeo.2011.03.012

Helz, G. R., Miller, C., Charnock, J., Mosselmans, J., Pattrick, R., Garner, C., & Vaughan, D. (1996). Mechanism of molybdenum removal from the sea and its concentration in black shales: EXAFS evidence. *Geochimica et Cosmochimica Acta*, *60*(19), 3631–3642. https://doi.org/10.1016/0016-7037(96)00195-0

Hong, W.-L., Lepland, A., Kirsimäe, K., Crémière, A., & Rae, J. W. B. (2022). Boron concentrations and isotopic compositions in methane-derived authigenic carbonates: Constraints and limitations in reconstructing formation conditions. *Earth and Planetary Science Letters*, *579*, 117337. https://doi.org/10.1016/j.epsl.2021.117337

Hu, Y., Feng, D., Chen, L., Zheng, G., Peckmann, J., & Chen, D. (2015). Using iron speciation in authigenic carbonates from hydrocarbon seeps to trace variable redox conditions. *Marine and Petroleum Geology*, *67*, 111–119. https://doi.org/10.1016/j.marpetgeo.2015.05.001

Hu, Y., Feng, D., Peckmann, J., Roberts, H. H., & Chen, D. (2014). New insights into cerium anomalies and mechanisms of trace metal enrichment in authigenic carbonate from hydrocarbon seeps. *Chemical Geology*, *381*, 55–66. https://doi.org/10.1016/j.chemgeo.2014.05.014

Huang, H., Wang, X., Gong, S., Krake, N., Jin, M., Li, N., et al. (2020). New constraints on the formation of hydrocarbon-derived low magnesium calcite at brine seeps in the Gulf of Mexico. *Sedimentary Geology*, *398*, 105572. https://doi.org/10.1016/j.sedgeo.2019.105572

Hutchings, A. M., Basu, A., Dickson, A. J., & Turchyn, A. V. (2020). Molybdenum geochemistry in salt marsh pond sediments. *Geochimica et Cosmochimica Acta*, *284*, 75–91. https://doi.org/10.1016/j.gca.2020.06.014

Jia, Z., Hu, Y., Bayon, G., Peckmann, J., Wang, X., Gong, S., et al. (2023). Raw data for "Seawater-Fluid composition records from molybdenum isotopes of Sequentially Extracted phases of Seep carbonate rocks" [Dataset]. Mendeley Data, V1. https://doi.org/10.17632/d95t3thrsz.1

Joye, S. B. (2020). The geology and biogeochemistry of hydrocarbon seeps. *Annual Review of Earth and Planetary Sciences*, *48*(1), 205–231. https://doi.org/10.1146/annurev-earth-063016-020052

Joye, S. B., Bowles, M. W., Samarkin, V. A., Hunter, K. S., & Niemann, H. (2010). Biogeochemical signatures and microbial activity of different cold-seep habitats along the Gulf of Mexico deep slope. *Deep-Sea Research: Topical Studies in Oceanography*, *57*(21–23), 1990–2001. https://doi.org/10.1016/j.dsr2.2010.06.001

Kendall, B., Dahl, T. W., & Anbar, A. D. (2017). The stable isotope geochemistry of molybdenum. *Reviews in Mineralogy & Geochemistry*, *82*(1), 683–732. https://doi.org/10.2138/rmg.2017.82.16

Li, J., Liang, X., Zhong, L., Wang, X., Ren, Z., Sun, S., et al. (2014). Measurement of the isotopic composition of molybdenum in geological samples by MC-ICP-MS using a novel chromatographic extraction technique. *Geostands and Geoanalytical Research*, *38*(3), 345–354. https://doi.org/10.1111/j.1751-908x.2013.00279.x

Liang, Q., Hu, Y., Feng, D., Peckmann, J., Chen, L., Yang, S., et al. (2017). Authigenic carbonates from newly discovered active cold seeps on the northwestern slope of the South China Sea: Constraints on fluid sources, formation environments, and seepage dynamics. *Deep Sea Research Part I: Oceanographic Research Papers*, *124*, 31–41. https://doi.org/10.1016/j.dsr.2017.04.015

Lin, Z., Sun, X., Strauss, H., Eroglu, S., Böttcher, M. E., Lu, Y., et al. (2021). Molybdenum isotope composition of seep carbonates – Constraints on sediment biogeochemistry in seepage environments. *Geochimica et Cosmochimica Acta*, *307*, 56–71. https://doi.org/10.1016/j.gca.2021.05.038

Luff, R., & Wallmann, K. (2003). Fluid flow, methane fluxes, carbonate precipitation and biogeochemical turnover in gas hydrate-bearing sediments at hydrate ridge, Cascadia margin: Numerical modeling and mass balances. *Geochimica et Cosmochimica Acta*, *67*(18), 3403–3421. https://doi.org/10.1016/S0016-7037(03)00127-3

Lumsden, D. S. (1979). Discrepancy between thin-section and X-ray estimates of dolomite in limestone. *Journal of Sedimentary Research*, *49*, 429–435. https://doi.org/10.1306/212F7761-2B24-11D7-8648000102C1865D

McManus, J., Nägler, T. F., Siebert, C., Wheat, C. G., & Hammond, D. E. (2002). Oceanic molybdenum isotope fractionation: Diagenesis and hydrothermal ridge-flank alteration. *Geochemistry, Geophysics, Geosystems*, *3*(12), 1078–1079. https://doi.org/10.1029/2002GC000356

Miller, C. A., Peucker-Ehrenbrink, B., Walker, B. D., & Franco, M. (2011). Re-assessing the surface cycling of molybdenum and rhenium. *Geochimica et Cosmochimica Acta*, *75*(22), 7146–7179. https://doi.org/10.1016/j.gca.2011.09.005

Morse, J. W., & Mackenzie, F. T. (1990). Geochemistry of sedimentary carbonates. In *Geochemistry of sedimentary carbonates*. Elsevier.

Naehr, T. H., Eichhubl, P., Orphan, V. J., Hovland, M., Paull, C. K., Ussler, W., et al. (2007). Authigenic carbonate formation at hydrocarbon seeps in continental margin sediments: A comparative study. *Deep Sea Research Part II: Topical Studies in Oceanography*, *54*(11–13), 1268–1291. https://doi.org/10.1016/j.dsr2.2007.04.010

Nägler, T. F., Anbar, A. D., Archer, C., Goldberg, T., Gordon, G. W., Greber, N. D., et al. (2014). Proposal for an international molybdenum isotope measurement standard and data representation. *Geostandards and Geoanalytical Research*, *38*(2), 149–151. https://doi.org/10.1111/j.1751-908X.2013.00275.x

Nägler, T. F., Neubert, N., Böttcher, M. E., Dellwig, O., & Schnetger, B. (2011). Molybdenum isotope fractionation in pelagic euxinia: Evidence from the modern Black and Baltic Seas. *Chemical Geology*, *289*(1–2), 1–11. https://doi.org/10.1016/j.chemgeo.2011.07.001

Neubert, N., Nägler, T. F., & Böttcher, M. E. (2008). Sulfidity controls molybdenum isotope fractionation into euxinic sediments: Evidence from the modern Black Sea. *Geology*, *36*(10), 775–778. https://doi.org/10.1130/G24959A.1

Niewöhner, C., Hensen, C., Kasten, S., Zabel, M., & Schulz, H. D. (1998). Deep sulfate reduction completely mediated by anaerobic methane oxidation in sediments of the upwelling area off Namibia. *Geochimica et Cosmochimica Acta*, *62*(3), 455–464. https://doi.org/10.1016/S0016-7037(98)00055-6

O'Sullivan, E. M., Nägler, T. F., Turner, E. C., Kamber, B. S., Babechuk, M. G., & O'Hare, S. P. (2022). Mo isotope composition of the 0.85 Ga ocean from coupled carbonate and shale archives: Some implications for pre-Cryogenian oxygenation. *Precambrian Research*, *378*, 106760. https://doi.org/10.1016/j.precamres.2022.106760

Peckmann, J., & Thiel, V. (2004). Carbon cycling at ancient methane-seeps. *Chemical Geology*, *205*(3–4), 443–467. https://doi.org/10.1016/j.chemgeo.2003.12.025

Phillips, R., & Xu, J. (2021). A critical review of molybdenum sequestration mechanisms under euxinic conditions: Implications for the precision of molybdenum paleoredox proxies. *Earth-Science Reviews*, *221*, 103799. https://doi.org/10.1016/j.earscirev.2021.103799

Pierre, C., Rouchy, J.-M., Blanc-Valleron, M.-M., Etoubleau, J., & Fouquet, Y. (2015). Methanogenesis and clay minerals diagenesis during the formation of dolomite nodules from the Tortonian marls of southern Spain. *Marine and Petroleum Geology*, *66*, 606–615. https://doi.org/10.1016/j.marpetgeo.2015.04.017

Poulson, R. L., Siebert, C., McManus, J., & Berelson, W. M. (2006). Authigenic molybdenum isotope signatures in marine sediments. *Geology*, *34*(8), 617–620. https://doi.org/10.1130/G22485.1

Poulton, S. W., & Canfield, D. E. (2005). Development of a sequential extraction procedure for iron: Implications for iron partitioning in continentally derived particulates. *Chemical Geology*, *214*(3–4), 209–221. https://doi.org/10.1016/j.chemgeo.2004.09.003

Roberts, H. H., Feng, D., & Joye, S. B. (2010). Cold-seep carbonates of the middle and lower continental slope, northern Gulf of Mexico. *Deep-Sea Research II: Topical Studies in Oceanography*, *57*(21–23), 2040–2054. https://doi.org/10.1016/j.dsr2.2010.09.003

Romaniello, S. J., Herrmann, A. D., & Anbar, A. D. (2016). Syndepositional diagenetic control of molybdenum isotope variations in carbonate sediments from the Bahamas. *Chemical Geology*, *438*, 84–90. https://doi.org/10.1016/j.chemgeo.2016.05.019

Rongemaille, E., Bayon, G., Pierre, C., Bollinger, C., Chu, N. C., Fouquet, Y., et al. (2011). Rare earth elements in cold seep carbonates from the Niger delta. *Chemical Geology*, *286*(3–4), 196–206. https://doi.org/10.1016/j.chemgeo.2011.05.001

Sato, H., Hayashi, K.-I., Ogawa, Y., & Kawamura, K. (2012). Geochemistry of deep sea sediments at cold seep sites in the Nankai Trough: Insights into the effect of anaerobic oxidation of methane. *Marine Geology*, *323*(325), 47–55. https://doi.org/10.1016/j.margeo.2012.07.013

Scholz, F., Siebert, C., Dale, A. W., & Frank, M. (2017). Intense molybdenum accumulation in sediments underneath a nitrogenous water column an implications for the reconstruction of paleo-redox conditions based on molybdenum isotopes. *Geochimica et Cosmochimica Acta*, *213*, 400–417. https://doi.org/10.1016/j.gca.2017.06.048

Schrag, D. P., Higgins, J. A., Macdonald, F. A., & Johnston, D. T. (2013). Authigenic carbonate and the history of the global carbon cycle. *Science*, *339*(6119), 540–543. https://doi.org/10.1126/science.1229578

Shields, G., & Veizer, J. (2002). Precambrian marine carbonate isotope database: Version 1.1. *Geochemistry, Geophysics, Geosystems*, *3*(6), 1–12. https://doi.org/10.1029/2001GC000266

Siebert, C., Nagler, T. F., & Kramers, J. D. (2001). Determination of molybdenum isotope fractionation by double-spike multicollector inductively coupled plasma mass spectrometry. *Geochemistry, Geophysics, Geosystems*, *2*(7), 1032. https://doi.org/10.1029/2000gc000124

Siebert, C., Nagler, T. F., von Blanckenburg, F., & Kramers, J. D. (2003). Molybdenum isotope records as a potential new proxy for paleoceanography. *Earth and Planetary Science Letters*, *211*(1–2), 159–171. https://doi.org/10.1016/S0012-821X(03)00189-4

Smrzka, D., Feng, D., Himmler, T., Zwicker, J., Hu, Y., Monien, P., et al. (2020). Trace elements in methane-seep carbonates: Potentials, limitations, and perspectives. *Earth-Science Reviews*, *208*, 103263. https://doi.org/10.1016/j.earscirev.2020.103263

Solomon, E. A., Kastner, M., Jannasch, H., Robertson, G., & Weinstein, Y. (2008). Dynamic fluid flow and chemical fluxes associated with a seafloor gas hydrate deposit on the northern Gulf of Mexico slope. *Earth and Planetary Science Letters*, *270*(1–2), 95–105. https://doi.org/10.1016/j.epsl.2008.03.024

Sun, Y., Feng, D., Smrzka, D., Peckmann, J., Huang, H., Roberts, H. H., & Chen, D. (2021). Uptake of trace elements into authigenic carbonate at a brine seep in the northern Gulf of Mexico. *Chemical Geology*, *582*, 120442. https://doi.org/10.1016/j.chemgeo.2021.120442

Sun, Y., Gong, S., Li, N., Peckmann, J., Jin, M., Roberts, H. H., et al. (2020). A new approach to discern the hydrocarbon sources (oil vs methane) of authigenic carbonates forming at marine seeps. *Marine and Petroleum Geology*, *114*, 104230. https://doi.org/10.1016/j.marpetgeo.2020.104230

Tessier, A., Campbell, P. G. C., & Bisson, M. (1979). Sequential extraction procedure for the speciation of particulate trace metals. *Analytical Chemistry*, *51*(7), 844–851. https://doi.org/10.1021/ac50043a017

Tong, H., Feng, D., Peckmann, J., Roberts, H. H., Chen, L., Bian, Y., & Chen, D. (2019). Environments favoring dolomite formation at cold seeps: A case study from the Gulf of Mexico. *Chemical Geology*, *518*, 9–18. https://doi.org/10.1016/j.chemgeo.2019.04.016

Tryon, M. D., Brown, K. M., Torres, M. E., Tréhu, A. M., McManus, J., & Collier, R. W. (1999). Measurements of transience and downward fluid flow near episodic methane gas vents, Hydrate Ridge, Cascadia. *Geology*, *27*(12), 1075–1078. https://doi.org/10.1130/0091-7613(1999)0272.3.CO;2

Voegelin, A. R., Nägler, T. F., Beukes, N. J., & Lacassie, J. P. (2010). Molybdenum isotopes in late Archean carbonate rocks: Implications for early Earth oxygenation. *Precambrian Research*, *182*(1–2), 70–82. https://doi.org/10.1016/j.precamres.2010.07.001

Voegelin, A. R., Nägler, T. F., Samankassou, E., & Villa, I. M. (2009). Molybdenum isotopic composition of modern and Carboniferous carbonates. *Chemical Geology*, *265*(3–4), 488–498. https://doi.org/10.1016/j.chemgeo.2009.05.015

Wang, J., Tarhan, L. G., Jacobson, A. D., Oehlert, A. M., & Planavsky, N. J. (2023). The evolution of the marine carbonate factory. *Nature*, *615*(7951), 265–269. https://doi.org/10.1038/s41586-022-05654-5

Wasylenki, L. E., Rolfe, B. A., Weeks, C. L., Spiro, T. G., & Anbar, A. D. (2008). Experimental investigation of the effects of temperature and ionic strength on Mo isotope fractionation during adsorption to manganese oxides. *Geochimica et Cosmochimica Acta*, *72*(24), 5997–6005. https://doi.org/10.1016/j.gca.2008.08.027

Wilkinson, B. H., & Walker, J. C. G. (1989). Phanerozoic cycling of sedimentary carbonate. *American Journal of Science*, *289*(4), 525–548. https://doi.org/10.2475/ajs.289.4.525

Zhao, M. Y., Zheng, Y. F., & Zhao, Y. Y. (2016). Seeking a geochemical identifier for authigenic carbonate. *Nature Communications*, *7*(1), 10885. https://doi.org/10.1038/ncomms10885

Zhao, P., Li, J., Zhang, L., Wang, Z., Kong, D., Ma, J., et al. (2016). Molybdenum mass fractions and isotopic compositions of international geological reference materials. *Geostands and Geoanalytical Research*, *40*(2), 217–226. https://doi.org/10.1111/j.1751-908X.2015.00373.x

Zheng, Y., Anderson, R. F., van Geen, A., & Kuwabara, J. (2000). Authigenic molybdenum formation in marine sediments: A link to pore water sulfide in the Santa Barbara Basin. *Geochimica et Cosmochimica Acta*, *64*(24), 4165–4178. https://doi.org/10.1016/S0016-7037(00)00495-6